March 2002 • NREL/SR-500-28719

Subcontractor Report

# Structural Health Monitoring Static Test of a Wind Turbine Blade

## August 1999

M.J. Sundaresan, M.J. Schulz, and A. Ghoshal
*Intelligent Structures and Mechanisms (ISM) Laboratory*
*Department of Mechanical Engineering*
*North Carolina A&T State University*
*Greensboro, North Carolina*

**National Renewable Energy Laboratory**

**1617 Cole Boulevard**
**Golden, Colorado 80401-3393**

**NREL is a U.S. Department of Energy Laboratory**
**Operated by Midwest Research Institute • Battelle • Bechtel**

**Contract No. DE-AC36-99-GO10337**

March 2002 • NREL/SR-500-28719

# Structural Health Monitoring Static Test of a Wind Turbine Blade

## August 1999

M.J. Sundaresan, M.J. Schulz, and A. Ghoshal
*Intelligent Structures and Mechanisms (ISM) Laboratory*
*Department of Mechanical Engineering*
*North Carolina A&T State University*
*Greensboro, North Carolina*

NREL Technical Monitor: A.S. Laxson

Prepared under Subcontract No. XCX-7-16469-01

**wable Energy Laboratory**

**1617 Cole Boulevard**
**Golden, Colorado 80401-3393**

**NREL is a U.S. Department of Energy Laboratory**
**Operated by Midwest Research Institute • Battelle • Bechtel**

**Contract No. DE-AC36-99-GO10337**

**NOTICE**



Available electronically at http://www.osti.gov/bridge

Available for a processing fee to U.S. Department of Energy
and its contractors, in paper, from:

U.S. Department of Energy
Office of Scientific and Technical Information
P.O. Box 62
Oak Ridge, TN 37831-0062
phone: 865.576.8401
fax: 865.576.5728
email: reports@adonis.osti.gov

Available for sale to the public, in paper, from:

U.S. Department of Commerce
National Technical Information Service
5285 Port Royal Road
Springfield, VA 22161
phone: 800.553.6847
fax: 703.605.6900
email: orders@ntis.fedworld.gov
online ordering: http://www.ntis.gov/ordering.htm

Printed on paper containing at least 50% wastepaper, including 20% postconsumer waste

# Summary


Structural health monitoring research is being performed by North Carolina A&T (NCA&T), the National Renewable Energy Laboratory (NREL) and Sandia Laboratories to develop a *smart blade.* A smart blade has an embedded sensor system integrated into the blade by the blade manufacturer. This sensor system will continuously monitor the condition of the blade, warn of initiating damage, and provide instant information that can be used to regulate the loading in the blade and reduce or prevent fatigue damage of the blade. This will reduce maintenance costs and improve the reliability of wind power. The collaborative research described in this report is a significant step in the development of the smart blade.

In the testing described herein, propagation characteristics of low frequency stress waves were evaluated for monitoring damage progression in an ERS-0100 wind turbine blade during proof testing. The structural health monitoring testing was performed during static testing of the blade and with the cooperation of the NREL, Sandia, and the blade manufacturer. This testing may be the first structural health monitoring testing performed on a full wind turbine blade during loading, and using the stress wave propagation technique. The health monitoring experiments were performed at the NREL test facility while the wind turbine blade was being quasi-statically loaded to failure. Bonded piezoceramic patches were used for generating and receiving the stress waves. The wind turbine blade failed by local buckling at 37.5% of the blade length measured from the root end, at a load level of 2053 kg (5500 lbs). Stress wave data were obtained up to a load level of 1680 kg (4500 lbs).

The raw signals received from sensors in the vicinity of the final failure showed recognizable changes in stress wave parameters. These changes occurred well ahead of the final failure. The stress wave data was processed using three different damage detection signal processing algorithms. All algorithms indicated a change in the structure with loading. Hence, stress wave propagation appears to have potential for the detection of evolving damage in composite structures such as wind turbine blades. This exploratory investigation needs to be followed with tests relating stress wave data to the damage initiation point and to progression of damage and buckling in the blade. These results could be used for early detection of damage and to possibly provide guidelines for design of the blade. Testing of other blades and investigation of the effects of compressive loading and bending on the propagation of stress waves should also be performed. Specific recommendations for further testing based on the stress wave data are given in the report.

# TABLE OF CONTENTS

# 1.0 Introduction

Moisture absorption, fatigue, wind gusts, and lightning strikes can damage wind turbine blades. In wind farms, aerodynamic interaction between different turbines can cause unpredictable and excessive loads on the blades. These stressors, as well as normal aerodynamic, or loads caused by changing gravity moments, cause fatigue damage to the blades. The blades are made from fiberglass, which is a cost-effective material for this application. However, because of the large size of the blades and the low specific modulus of fiberglass, the blades' natural frequencies are low. Under loading, the deflections and strains of the cantilevered blade can be quite large making fatigue life an important design consideration. If fatigue damaged rotor blades fail, they can cause catastrophic damage to a wind turbine. While the design lifetime for blades is from 10 to 30 years, predicting the exact fatigue life is difficult. In addition, it is difficult to tell the extent of fatigue damage that might have occurred to a blade. Thus, a method is needed to continuously monitor the condition of the blade and warn of possible failure.

Health monitoring of the rotor blades and timely identification of potential failure areas can prevent failure of the entire horizontal axis wind turbine. A health monitoring system integrated within the blade could locate blade failures, reducing wind turbine life-cycle costs and the costs of energy. These blade failures sometimes occur near the root section or in the third of the blade near the root. Buckling of the surface of the blade at the maximum chord section is one type of failure. When this buckling occurs, the blades may operate for a large number of cycles with little reduction in strength and elastic properties, and then the fatigue damage propagates quickly to failure. The health monitoring technique proposed is a condition-based maintenance program that would monitor the condition of the blades during operation, or in the field when the turbine is stopped. Structural health monitoring (SHM) information will minimize the time needed for inspection of components. In addition, this technique will prevent unnecessary replacement of components, prevent failures, and allow utility companies to count on the availability of power. Structural health maintenance may also allow the use of lighter blades that would provide higher performance with less conservative margins of safety.

North Carolina A&T (NCA&T) researchers have detected minor damage sites in structures [1-30] using stress wave and other structural health monitoring techniques. Other researchers [31-39] have also developed damage detection techniques. It is anticipated these methods can detect damage in operational wind turbine blades before the damage sites can combine and propagate to cause failure of the blade. Some SHM techniques consider flat uniform panels with closely spaced sensor/actuator elements. However, an SHM system that monitors wind turbine blades considering thick structural sections, a complex built-up structure with curvature, and use of a minimum number of sensor/actuator elements must be designed. Current methods use a set of piezoceramic patches to generate and propagate stress waves through critical regions of the blade. After propagation through the critical zones, the stress waves are intercepted and measured using another set of piezoceramic patches or other sensors. This report is an exploratory study in which the evolving damage to a blade was monitored during a structural proof test using piezoceramic patch actuators and sensors.

The ERS-0100 wind turbine blade is a composite construction. Modifications to an earlier design were to be verified for strength by this static test. Researchers from the National Renewable Energy Laboratory (NREL), Sandia National Laboratories (Sandia), Physical Acoustics, and NCA&T conducted testing on the blade at the NREL facility in Golden, Colorado. Sandia and Physical Acoustics personnel collected acoustic emission data; NREL personnel collected strain data; and the NCA&T research engineer collected stress wave propagation data related to damage progression as the blade was loaded.

The objective of the work was to determine if damage occurring to the wind turbine blade during the test loading cycle could be detected by propagating stress waves through critical sections of the blade.

Damage would be identified by comparing stress wave parameters as loading is increased. The testing was exploratory in nature because it was the first attempt at monitoring structural damage using this approach on a full-scale blade during loading.

# 2.0 Test Configuration

This section describes the test setup and instrumentation used in the experiment.

### *2.1 Blade Geometry*

The approximate shape of the blade and the locations of the piezoceramic (PZT) patches bonded to the blade are shown in Figure 1. The blade was 9 m (29.5 ft) long with a maximum chord width of 1034 mm (40.7 in). The blade shell consisted of a shear web, unidirectional spar caps, a high-pressure skin section, a low-pressure skin section, and balsa wood coring (Figure 1). The spar cap regions around the axial locations of 37.5% and 72% of blade length were expected to be the critical regions based on testing of earlier blades. These regions were monitored through stress wave propagation. The PZT patches were bonded above the top spar caps. The detailed locations of the PZT patches are shown in Figure 1c. The patches were bonded using a standard strain gage bonding procedure using the M-Bond strain gage adhesive. The cross-sectional geometry of the blade is shown in Figure 2.

### *2.2 Loading*

The blade was loaded using a waffle tree arrangement, in which a single point load applied through a calibrated load cell was divided into four individual loads. These loads were applied at axial locations corresponding to 50%, 65%, 80%, and 90% of length measured from the root end. The loading arrangement is shown in Figure 3.

## *2.3 Instrumentation*

Piezoceramic patches, part QP10N from ACX Inc. [40], were used for transmitting, as well as receiving, the stress waves. The patches were 5.08 cm (2 in) long, 2.54 cm (1 in) wide, and 0.038 cm (0.015 in) thick. The patches were installed only on the top surface of the blade because this area is subjected to compression during the static loading cycle. The patches were oriented with their 2 inch length along the chord direction of the blade. No patches were used on the lower side of the blade because the PZT patches were not expected to survive the high tensile strains seen on that surface. The PZT patches were located above the shear web and the unidirectional spar cap on the top surface of the blade. Hence, it is likely that the stress wave responses will be most sensitive to the damage initiating in the spar cap and the skin above the spar cap. Stress waves were significantly attenuated by the Balsa wood being bonded to the low-pressure section of the skin. Stress waves were generated and monitored using a portable instrumentation system built of commercial components by NCA&T. A schematic of the instrumentation system is shown in Figure 4. Signals were generated using an HP 33120A arbitrary function generator. These signals were amplified using two ACX single channel power amplifiers and then used to excite the transmitting patches T1 and T2 (Figure 1). Two receiving patches were located on either side of these transmitters. The distance between the transmitters and receivers was based on both the space limitations between the load saddles and the expected failure points. The distance between the transmitters and receivers at the two locations was different because of constraints imposed by the loading arrangement. The signals received from the patches R1 to R4 (Figure 1) were digitized using a LeCroy 9304 digital oscilloscope. Data was downloaded to the hard drive of a laptop computer. The oscilloscope was set to start the waveform acquisition based on reaching the trigger level of the response in channel 1. Approximately 30 strain gages and 20 acoustic emission sensors were installed and monitored on the blade by NREL, Sandia and Physical Acoustics researchers. Some strain gage data were used in interpreting the stress wave results. This data is discussed in the following sections.

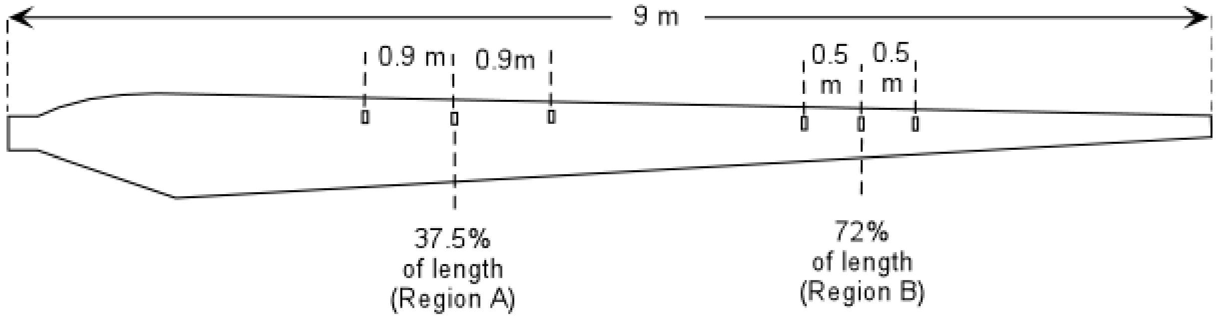


**a.** Plan view of the blade showing the locations of the PZT patches

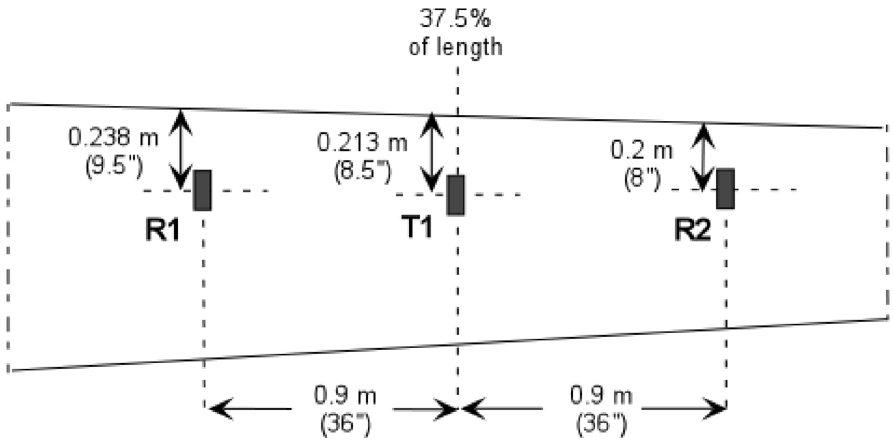


**b.**Transmitters and receivers in region A

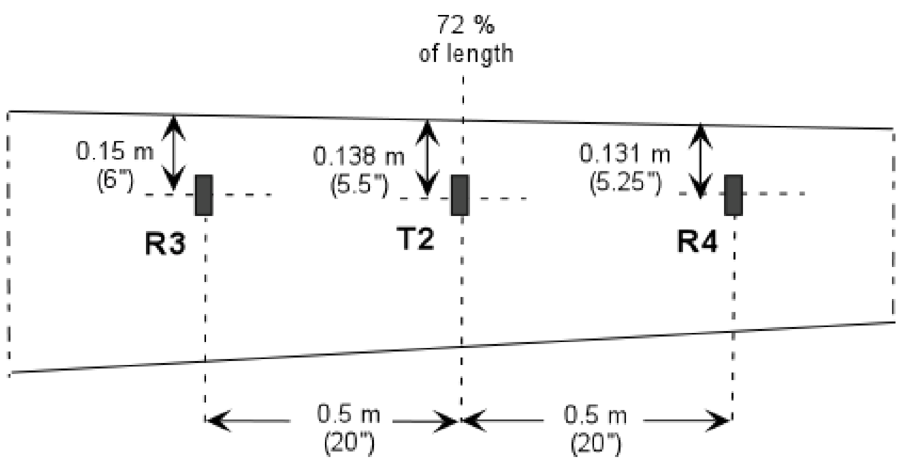


**c.** Transmitters and Receivers in region B

**Figure 1. Wind turbine blade plan view geometry and PZT patch locations**

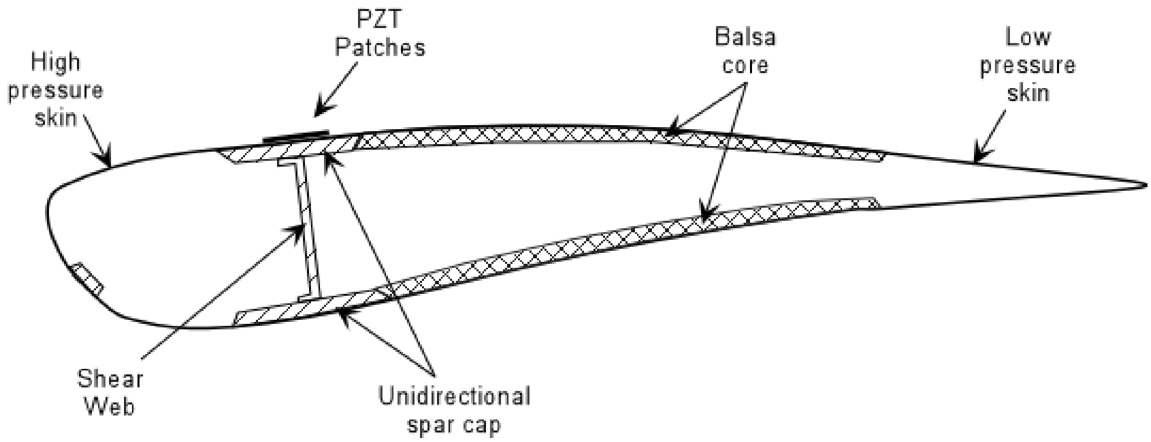


**Figure 2. Wind turbine blade cross-sectional geometry and PZT patch locations**

**Figure 3. The instrumented blade showing the loading arrangement**

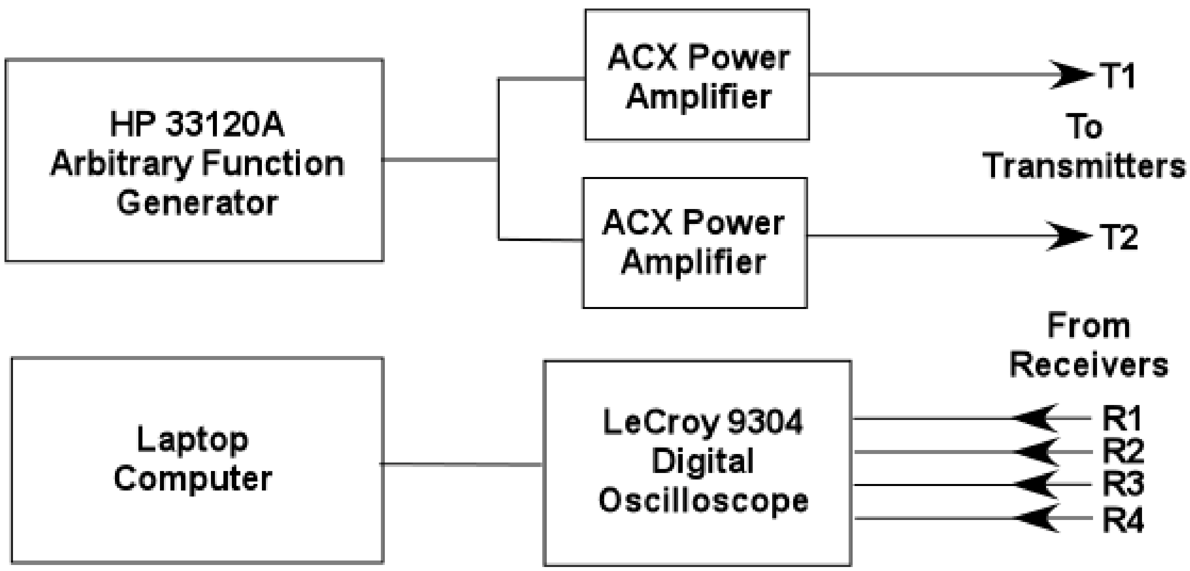


**Figure 4. Instrumentation used for monitoring stress wave propagation on the blade**

## 3.0 Test Results and Discussion

Stress wave signals were evaluated prior to the actual test by transmitting signals across the test section using the bonded PZT patches. Different frequencies and burst lengths were used. Frequencies ranging from 1 kHz to 20 kHz were examined. Based on these initial experiments, and to keep the comparison of signals at different frequencies simple, tone bursts lasting 7 to 10 complete sine wave cycles were used. The signals received that corresponded to the undamaged blade at various frequencies using tone bursts with 10 cycles are shown in Figures 5a—5d. The transmission distance at location A was nearly double the transmission distance in location B. The cross section of the blade at point A was much larger than the blade section at point B. This caused the signal amplitude at location A to be smaller than the signal amplitude at point B. When the signal frequency is increased from 3 kHz to 10 kHz, there is a decrease in the signal amplitude. This is because, for a given power input, the vibration displacement amplitude of a structure decreases with frequency, except at resonant frequencies. Further, the received tone bursts have distorted waveforms, and the level of distortion varies as a function of the frequency. This is because more than one mode can be excited and there is dispersion in propagating waves where the higher frequency waves can travel faster than the low frequency waves. In this experiment, a rectangular window and a sine wave were used for excitation, and the excitation frequency was chosen to give sufficient amplitude of response at the receivers. During the load cycle, researchers had only a few seconds to stop the load and obtain the stress wave readings. For this reason, a tone burst containing 7 cycles at 5 kHz was used.

Tone bursts containing 7 cycles at 5 kHz were obtained during the test at load levels ranging from zero load to 4500 lbs. Figures 6a to 6d show the waveforms corresponded to the four sensors at different load levels. The final failure occurred at an axial location approximately 37.5% from the root end near the transmitting sensor T1. The maximum load reached was approximately 5500 lbs. The deformed shape of the blade during loading is shown in Figure 7. The location of the failure in the blade is shown in Figure 8. The buckling occurred near T1 between T1 and R1. No apparent damage was seen at any other location on the blade length. Strain data from the neighborhood of the T1 and T2 transmitters was examined as a means to quantify the evolving damage in the blade. This data is shown in Figure 9a and 9b. Some nonlinearity in the load strain plot is seen at approximately 2500-lb. load. However, significant deviation from linear response in the strain data occurred around 4000 lbs. This strain data is also an indicator of damage because the strain gage in this case is at the damage site. Because strain is a very localized measurement, in general, a large number of strain gages would be required to monitor a structure for damage. This is in contrast to the stress wave technique that uses wave propagation through the structure to detect damage using a small number of channels of data acquisition.

The test results show that stress wave parameters are sensitive to the evolving structural damage occurring in the blade. The stress wave amplitudes from sensors R1 to R4 (Figure 6) were examined at different load levels. The relative time of arrival of these four signals could be directly compared because the oscilloscope sweeps of the signals were triggered at the same instant. The amplitude and the waveform of the stress wave signals changed as the load level was increased. Maximum changes occurred near the failure of the blade. Significant changes in the amplitude were seen in receivers R1 and R4 at the 4000-lb. load. The amplitude remained the same or slightly increased with the load level for receivers R2 and R3. The arrival time of the second peak after the trigger point for receiver R-1 was delayed by approximately 7 microseconds when the load level was increased to 4000 lbs. (Figure 6a). However, subsequent peaks did not show additional delays. Similar shifts were also seen in signals from the other three sensors, with the maximum shift occurring for sensor R2. The changing geometry of the blade due to bending during the test may also have affected the stress wave propagation. The waveforms show a phase delay in all receivers. However, the delay goes to zero after about one millisecond for receiver R1. This may be due to reflection of the wave from transmitter T1 at the root end of the blade and a combination of the transmitted and reflected signals at receiver R1. The other three receivers have outboard load saddles. The load saddles have foam against the blade that attenuates the stress waves and they do not reflect. Thus, their phase delay remains for the entire signal period. The stress in the actuators and sensors also changed with loading and this will have some effect on the wave sensing. As the blade curvature increases, the preload strain in the piezoceramic patches will increase. This may require that a larger level of excitation signal reach the receiver patches to trigger the data acquisition. This may cause a phase change in recording the waveforms. As a cantilever bar becomes curved, it will become stiffer. The lower natural frequencies of the bar will increase with curvature and the wavelength of the modes will decrease. The velocity of propagation of flexural waves in a bar increases with decreasing wavelength up to a point at which it becomes constant. This indicates that the wave speed would increase or stay the same as the blade increases in curvature. However, all of these effects must be verified by modeling and testing. To partly compensate for the curvature effect, the experimentation is done at higher frequencies, and an exciter patch is used with two outboard receiver patches equally spaced from the generator patch. Comparison of the responses of the two receiver patches will indicate any nonsymmetric damage about the generator patch. This approach can propagate waves long distances and damage can be detected using a small number of patches and channels of data acquisition. Also, experimentation by loading and reloading the blade can quantify the effect of blade curvature, and wave propagation signals can be saved for different load levels. The geometry and stress effects may then be removed from the waveforms leaving the damage effects.

In this exploratory study, changes in the signal amplitude and relative phase were seen in the received signal, particularly near the final failure of the blade. The blade is a closed tube that has multiple paths for the propagation of the transmitter and receiver stress waves. The shortest distances between the transmitters and the respective receivers are along the line joining them. The changes occurring in the material properties along this path are likely to have the greatest effect on the received signals. Balsa wood bonded to the low-pressure skin of the blade is highly attenuated, making stress waves travel difficult. The high-pressure skin, spar cap, and shear web are in the vicinity of this propagation path. Changes occurring to these components are likely to affect the received signal characteristics.

These empirical observations need to be substantiated with additional detailed experiments and analysis. For example, detailed failure analysis of the blade would be helpful in correlating the changes in the stress waves with the local failure modes of the blade. One of the likely precursors to the final failure modes is the local buckling of the shear web (Figure 10). If the failure analysis confirms this to be the failure mode, then monitoring the shear web directly by bonding patches on it would be advantageous. (See the Appendix for additional figures showing the blade and sensor responses.)

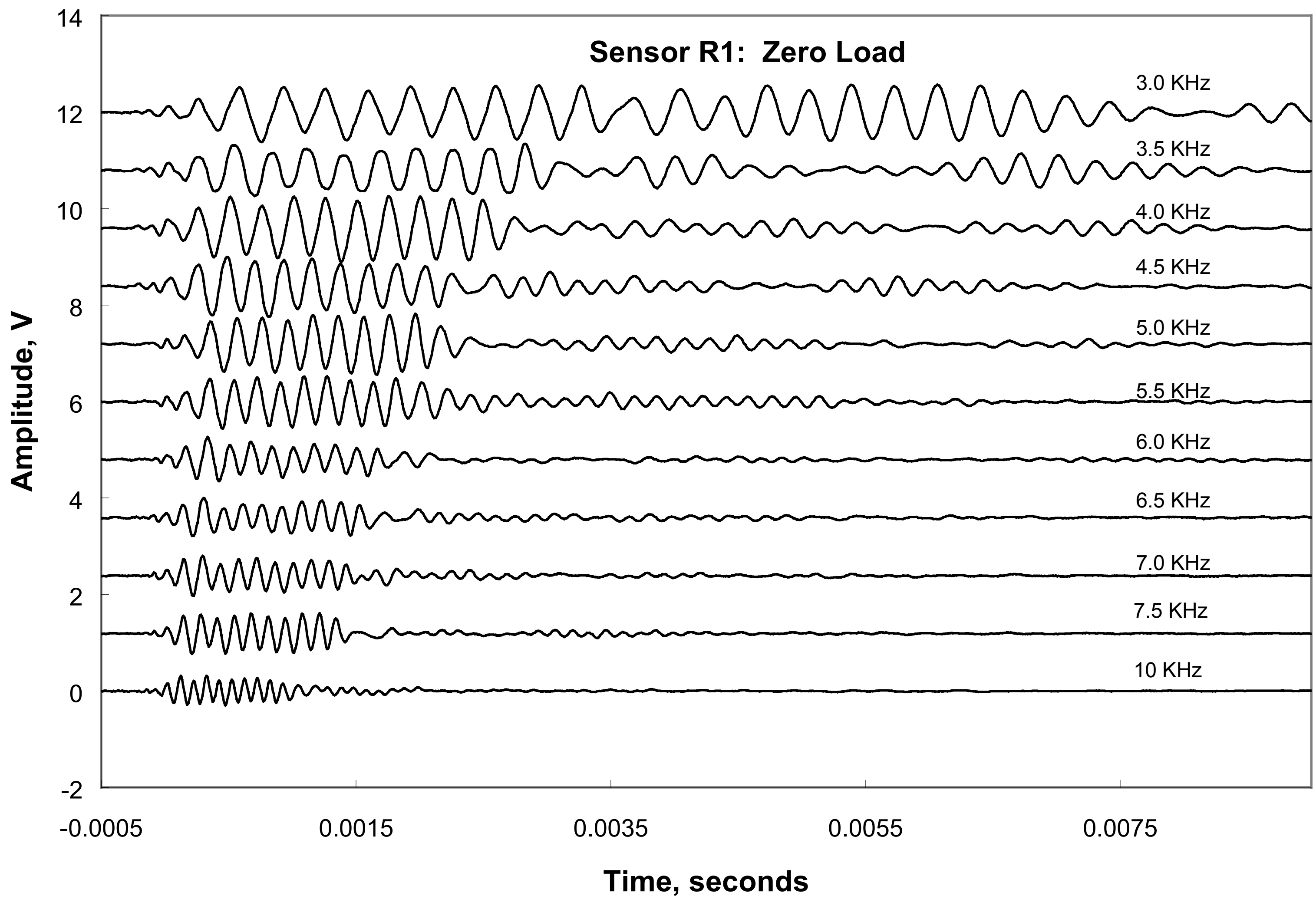


**Figure 5a. Stress waves received by sensing patch R1 at zero load, corresponding to sine wave tone bursts consisting of seven cycles of 200 V peak to peak from transmitting patch T1 at various input frequencies**

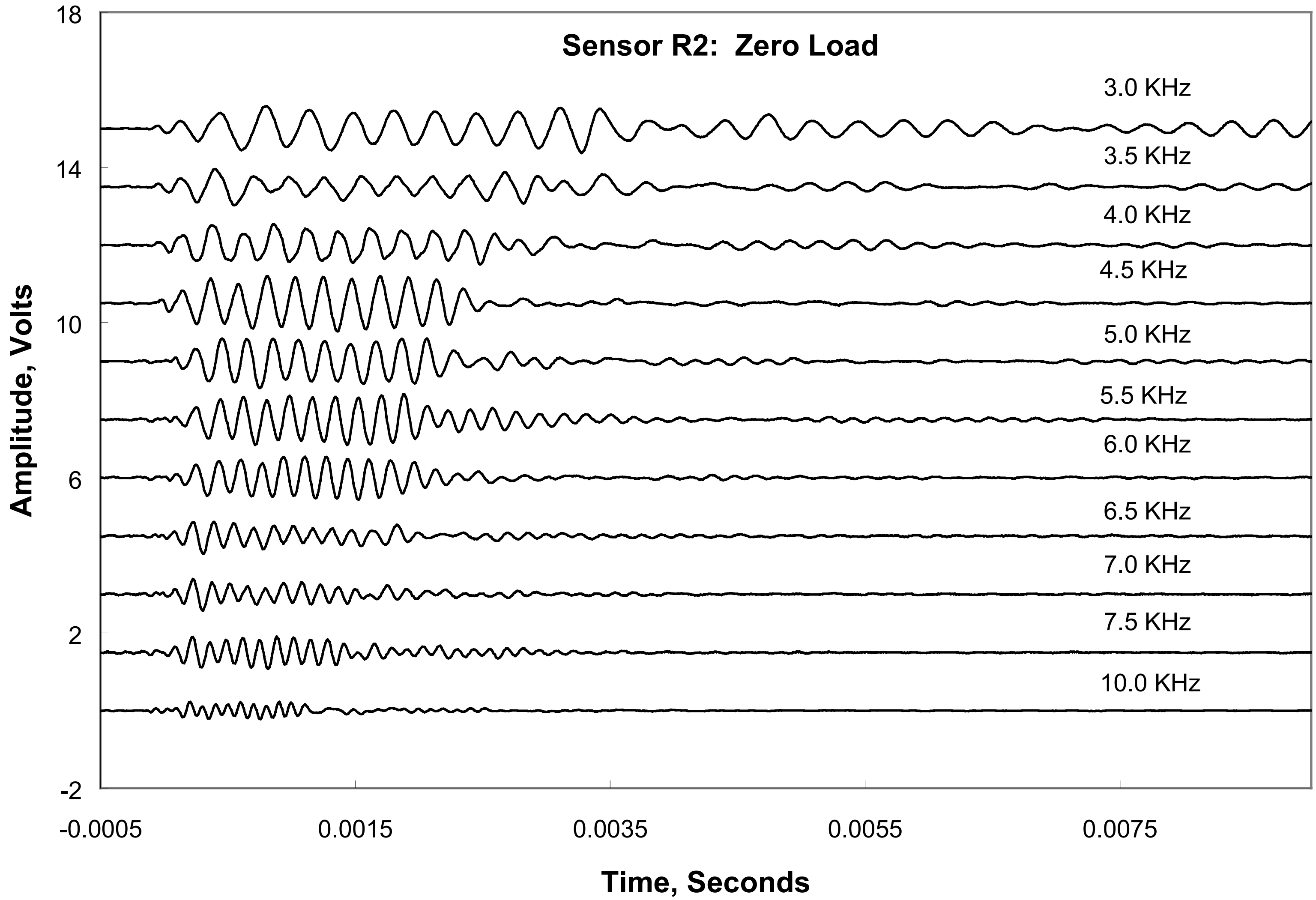


**Figure 5b. Stress waves received by sensing patch R2 at zero load, corresponding to sine wave tone bursts consisting of seven cycles of 200 V peak to peak from transmitting patch T1 at various input frequencies**

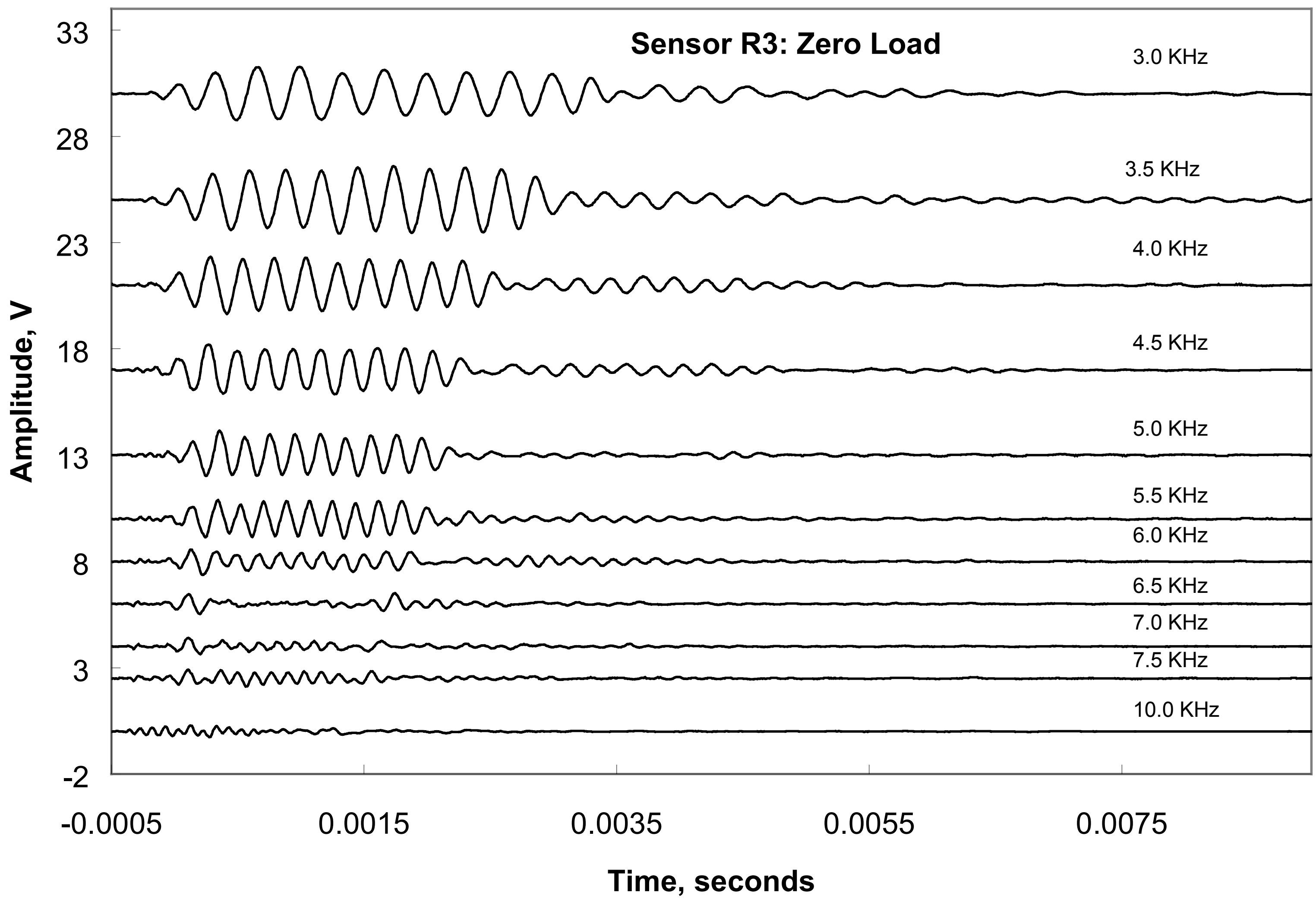


**Figure 5©. Stress waves received by sensing patch R3 at zero load, corresponding to sine wave tone bursts consisting of seven cycles of 200 V peak to peak from transmitting patch T2 at various input frequencies**

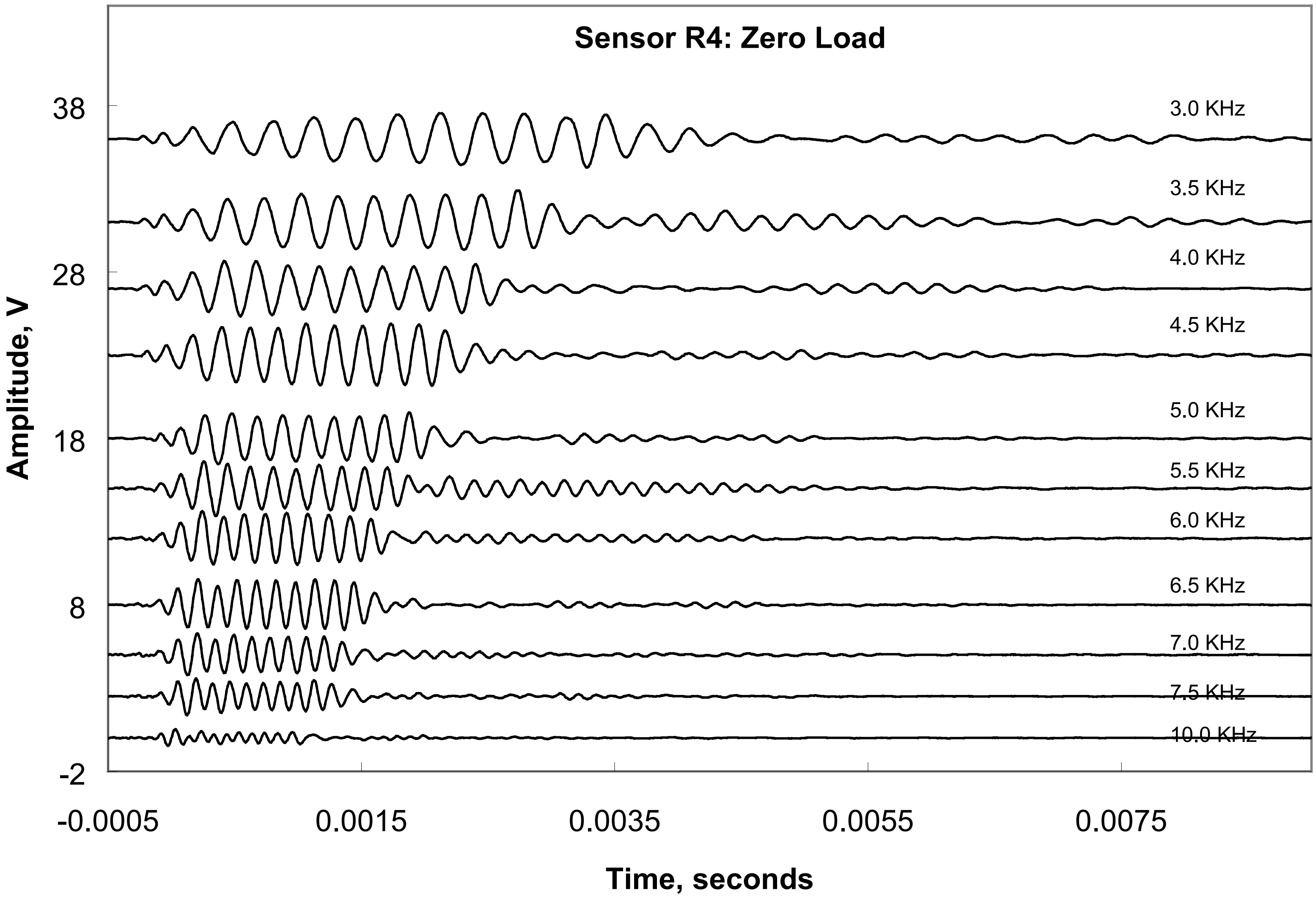


**Figure 5d. Stress waves received by sensing patch R4 at zero load, corresponding to sine wave tone bursts consisting of seven cycles of 200 V peak to peak from transmitting patch T2 at various input frequencies**

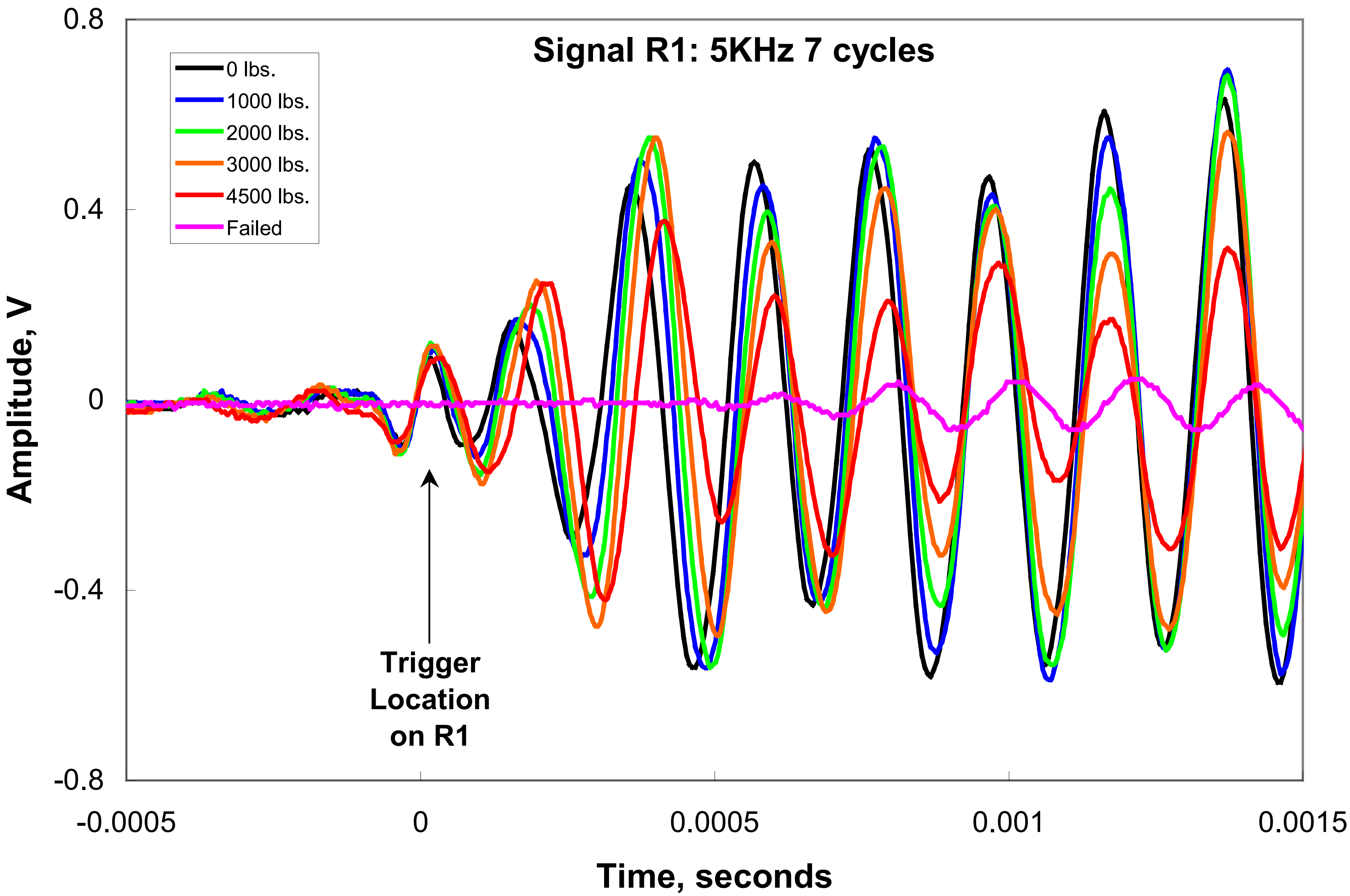


Figure 6a. The waveform from sensor R1 at different load levels

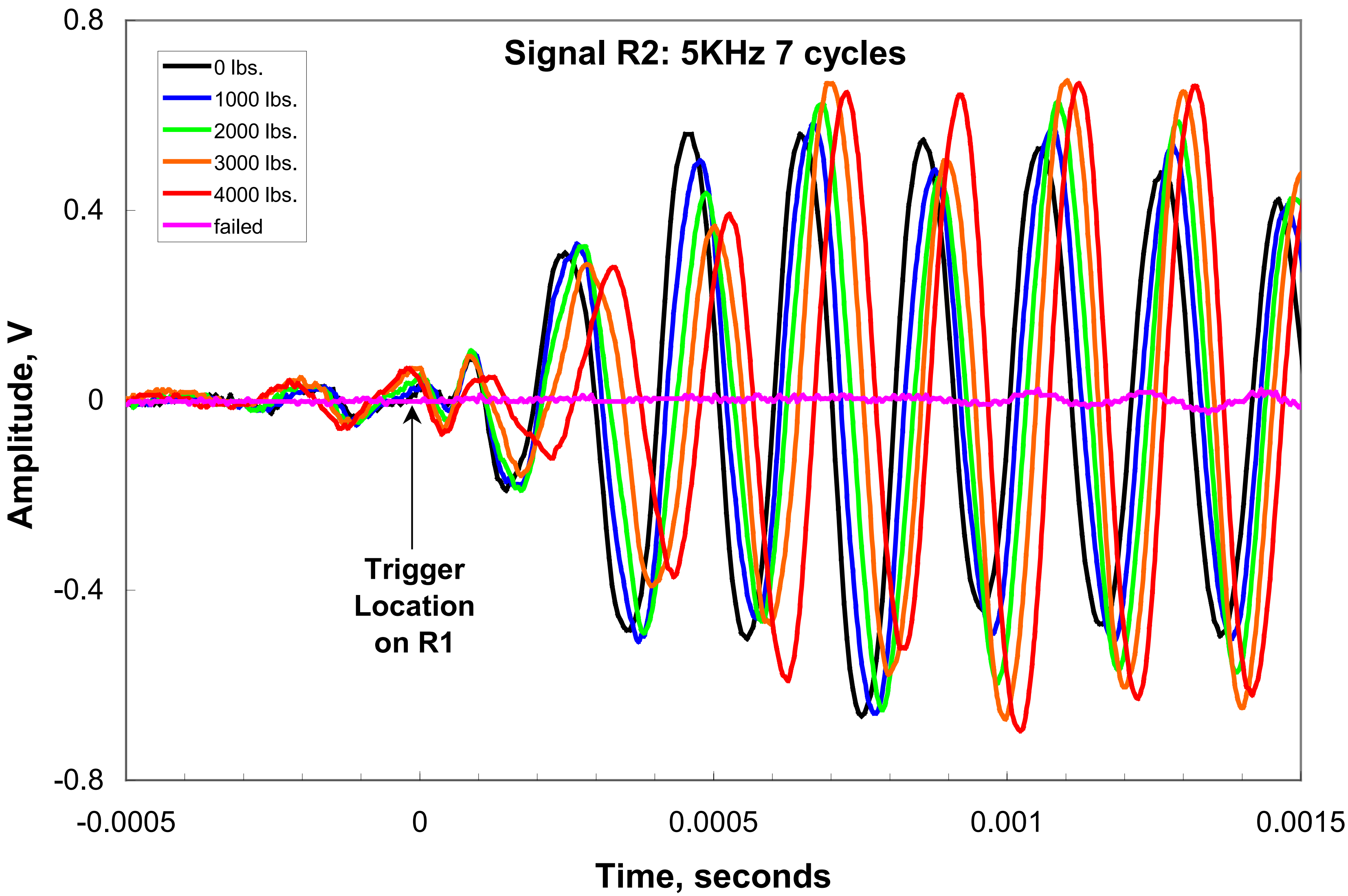


**Figure 6b. The waveform from sensor R2 at different load levels**

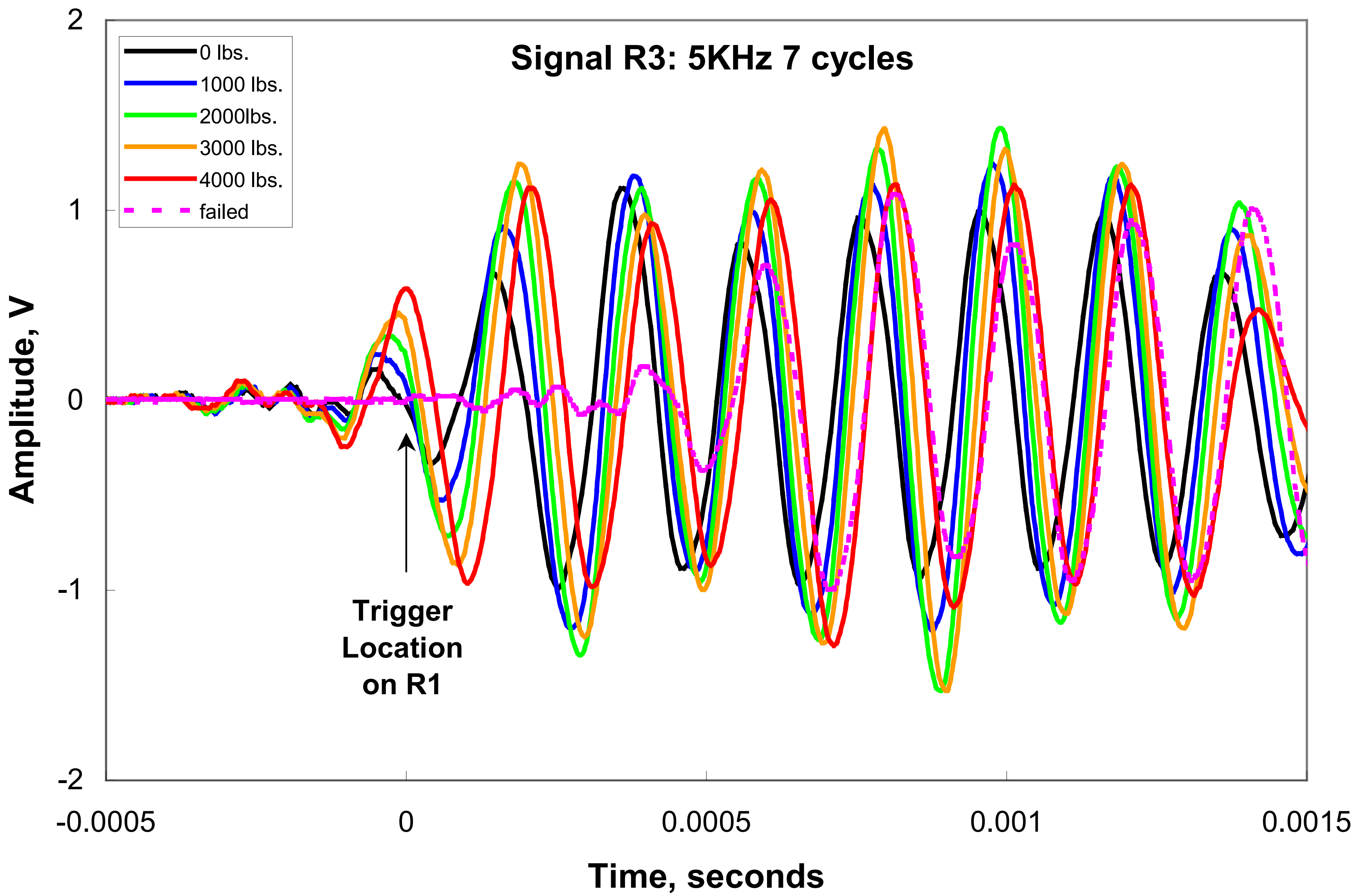


**Figure 6c. The waveform from sensor R3 at different load levels**

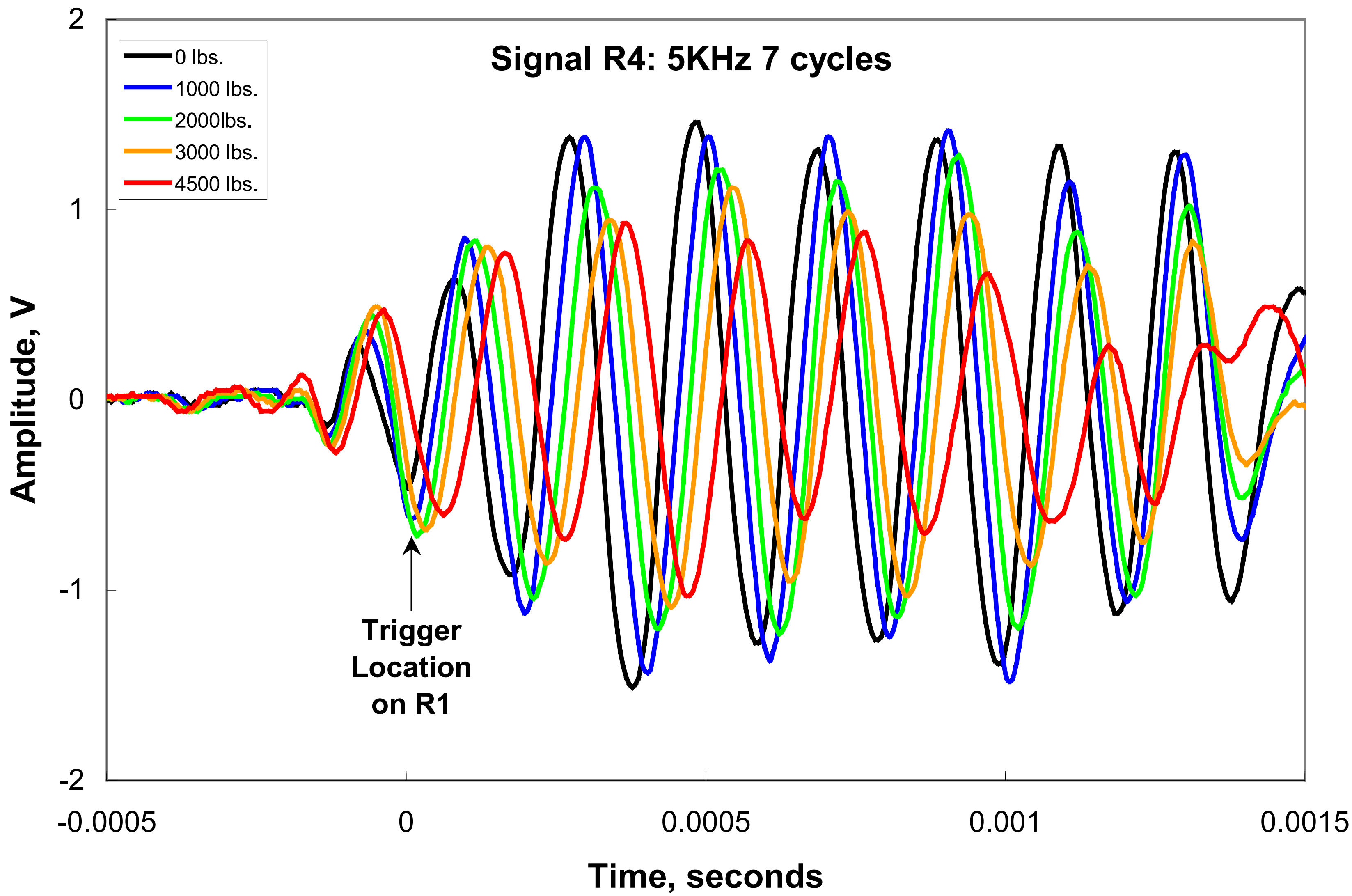


**Figure 6d. The waveform from sensor R4 at different load levels**

**Figure 7. The deformed shape of the blade during loading**

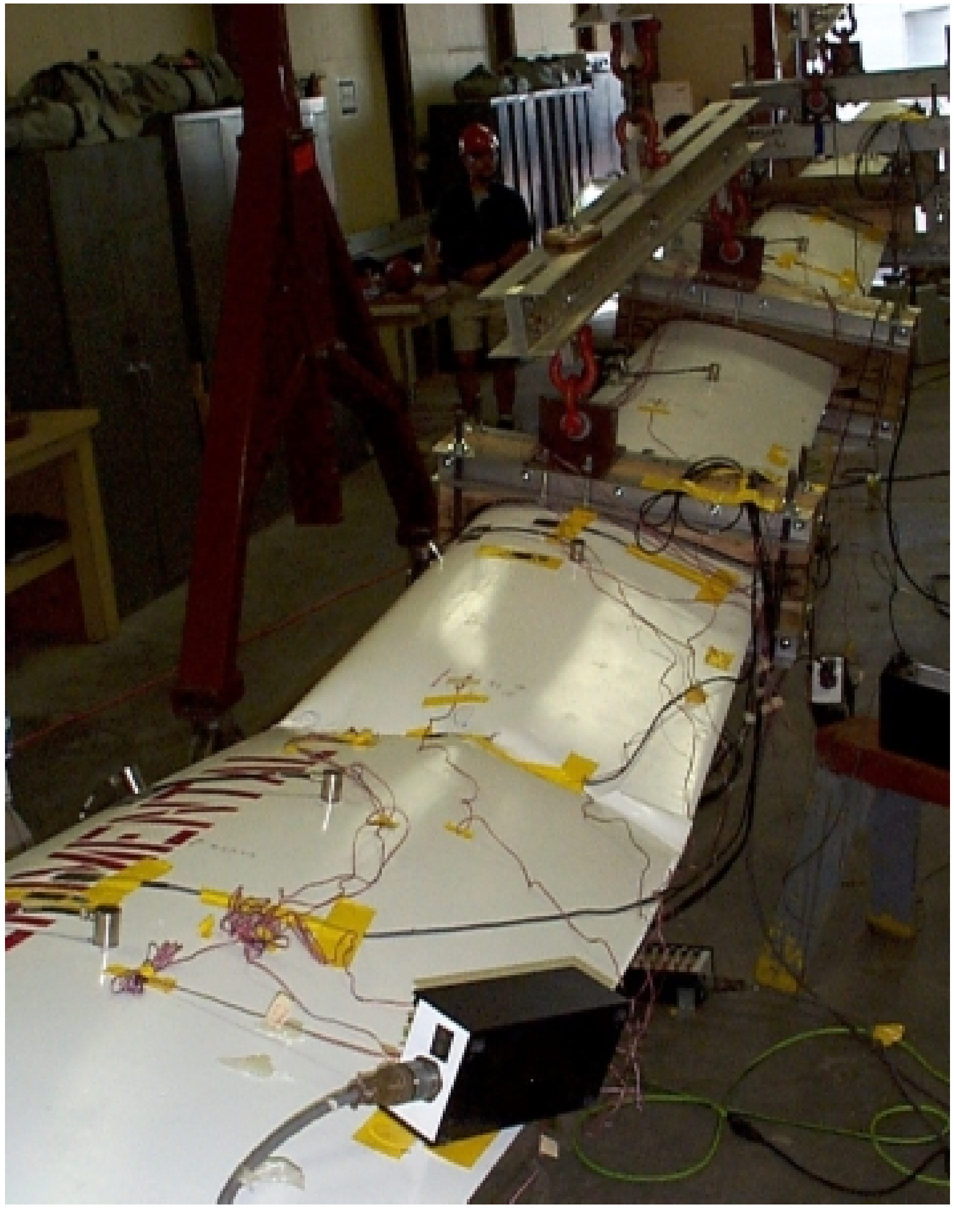

**Figure 8. Failed blade as viewed from the root end**

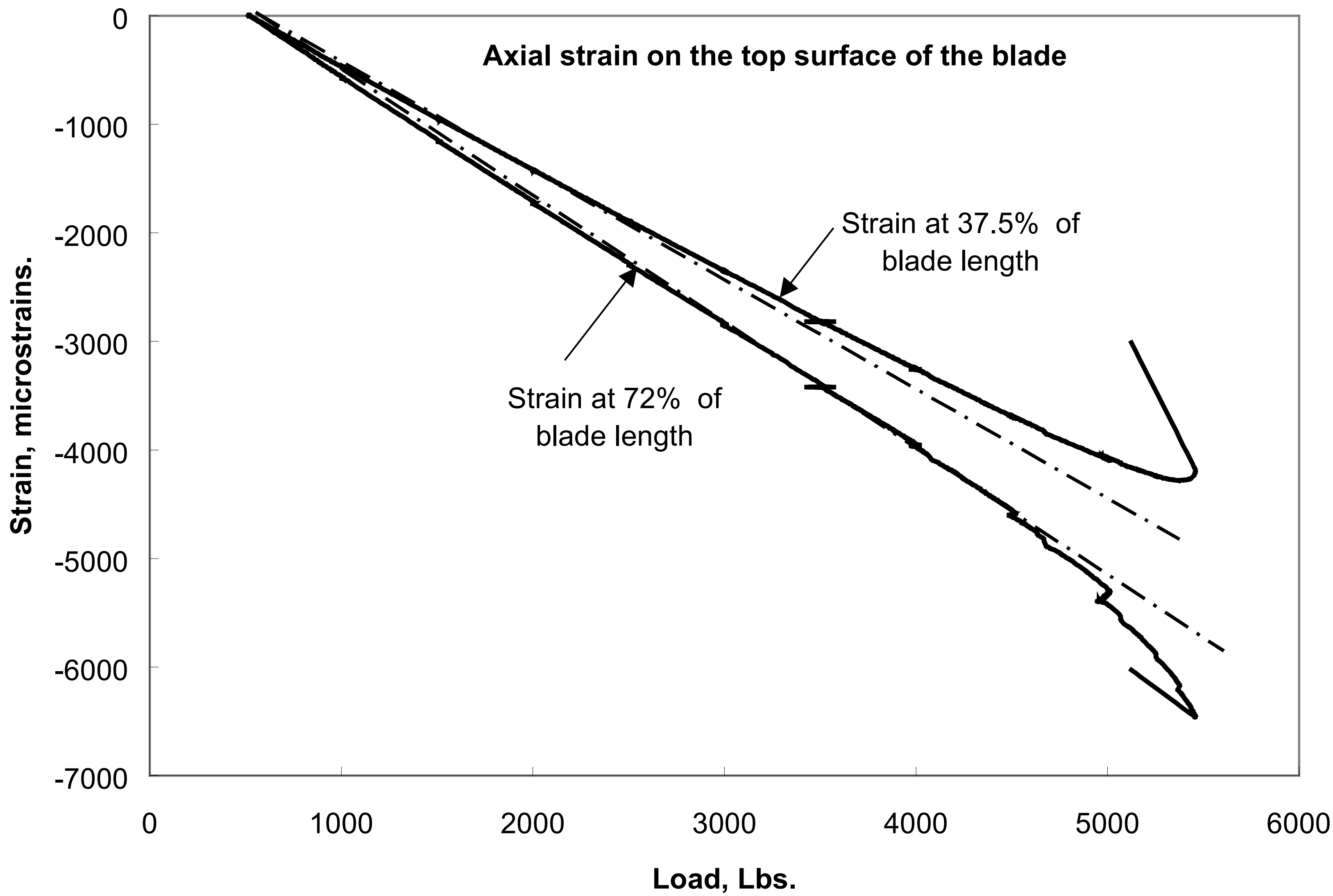


**Figure 9a. Axial strain on the top surface of the blade at the critical regions of the blade**

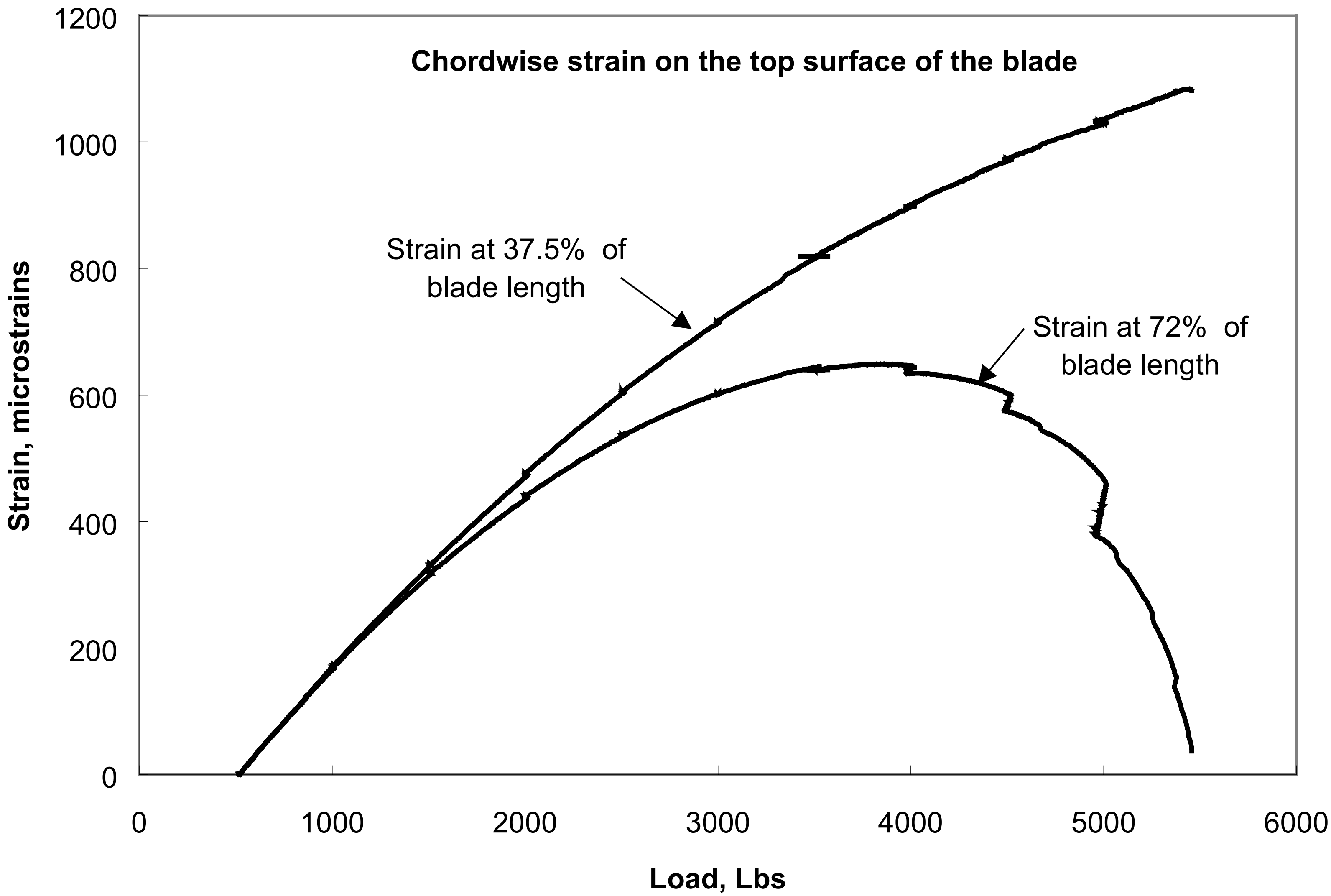


**Figure 9b. Chordwise strain on the top surface of the blade at the critical regions of the blade**

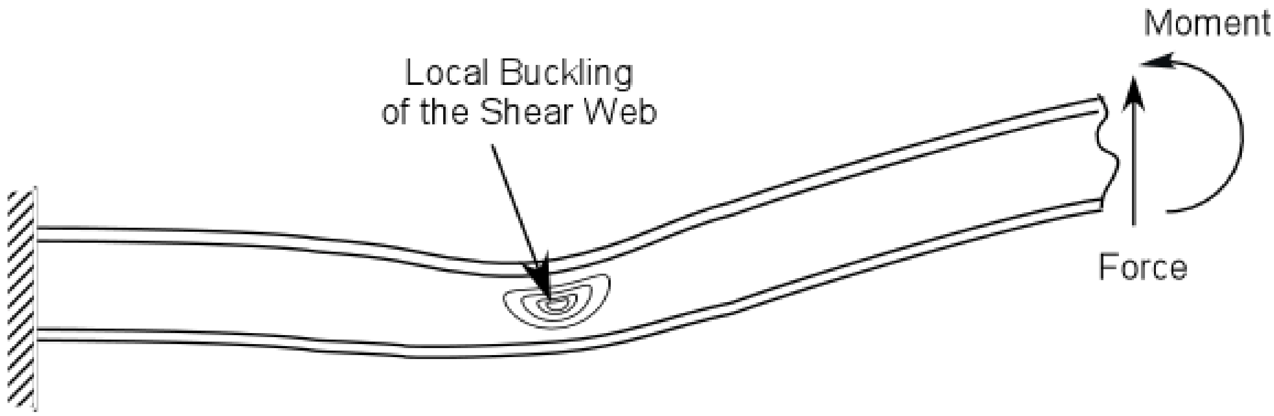


**Figure 10. One possible failure mode of the blade by local buckling of the shear web**

## 4.0 Damage Detection Analyses

Damage detection algorithms are used to provide a measure of damage evolution. Before computing the damage detection indicators, a change in the structure or damage can be observed by comparing Figure 11, which shows all four receiver waveforms at zero load, and Figure 12, which shows the four receiver waveforms at 4,000 lb. load. Figure 11 shows all four receiver waveforms at zero load, while Figure 12 shows the four receiver waveforms at 4000-lb. load. These significant changes in phase and amplitude indicate that the structure has changed. Three independent methods for damage detection developed at NCA&T University are used to predict if damage will occur to the blade: (1) the resonant comparison method, (2) the variance method, and (3) the wavelet pattern recognition method. These damage detection methods provide a metric that indicates change or damage in the structure. An array of sensors and the damage vector or other algorithms could potentially provide information on damage size and the damage force magnitude. Two frequency domain methods for damage detection, the transmittance function method and damage vector method, have not been tested with this data.

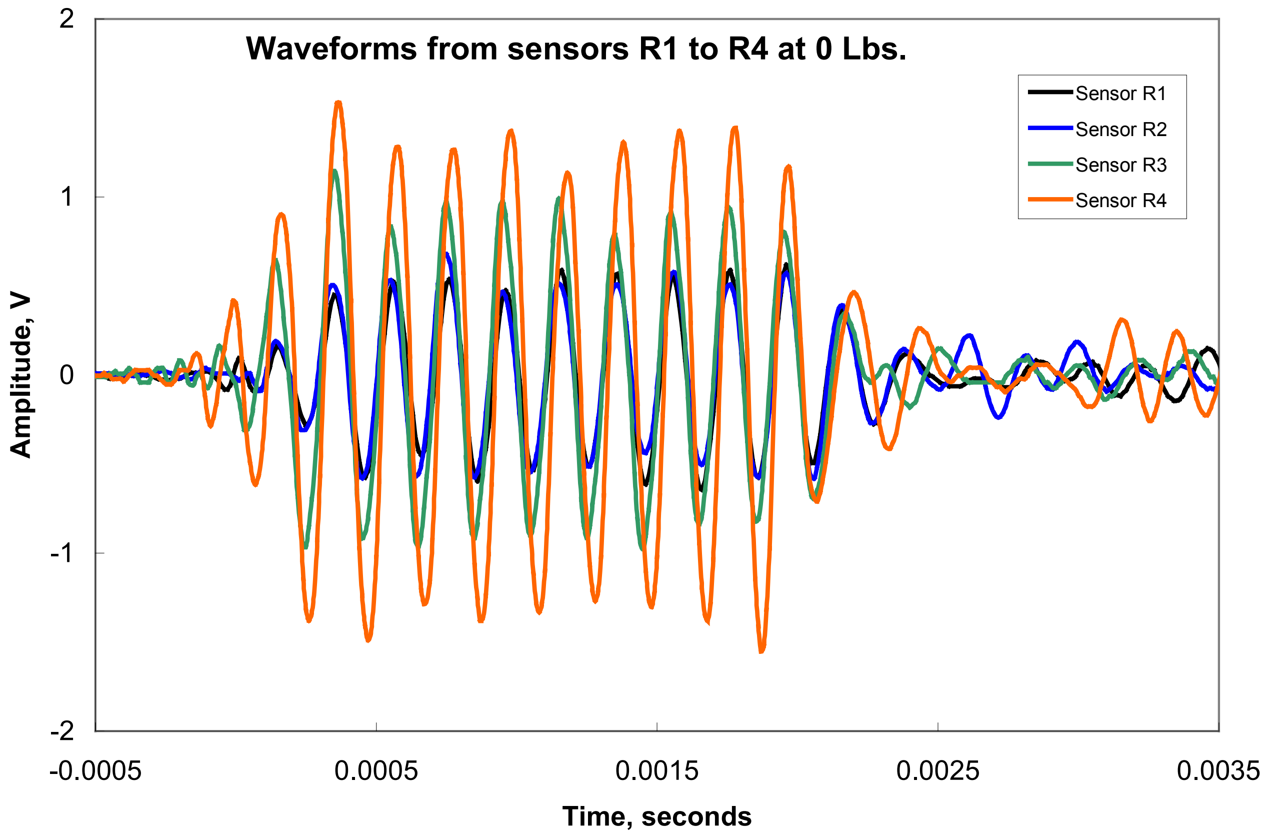


**Figure 11. Comparison of waveforms from sensors R1 to R4 for the no load condition**

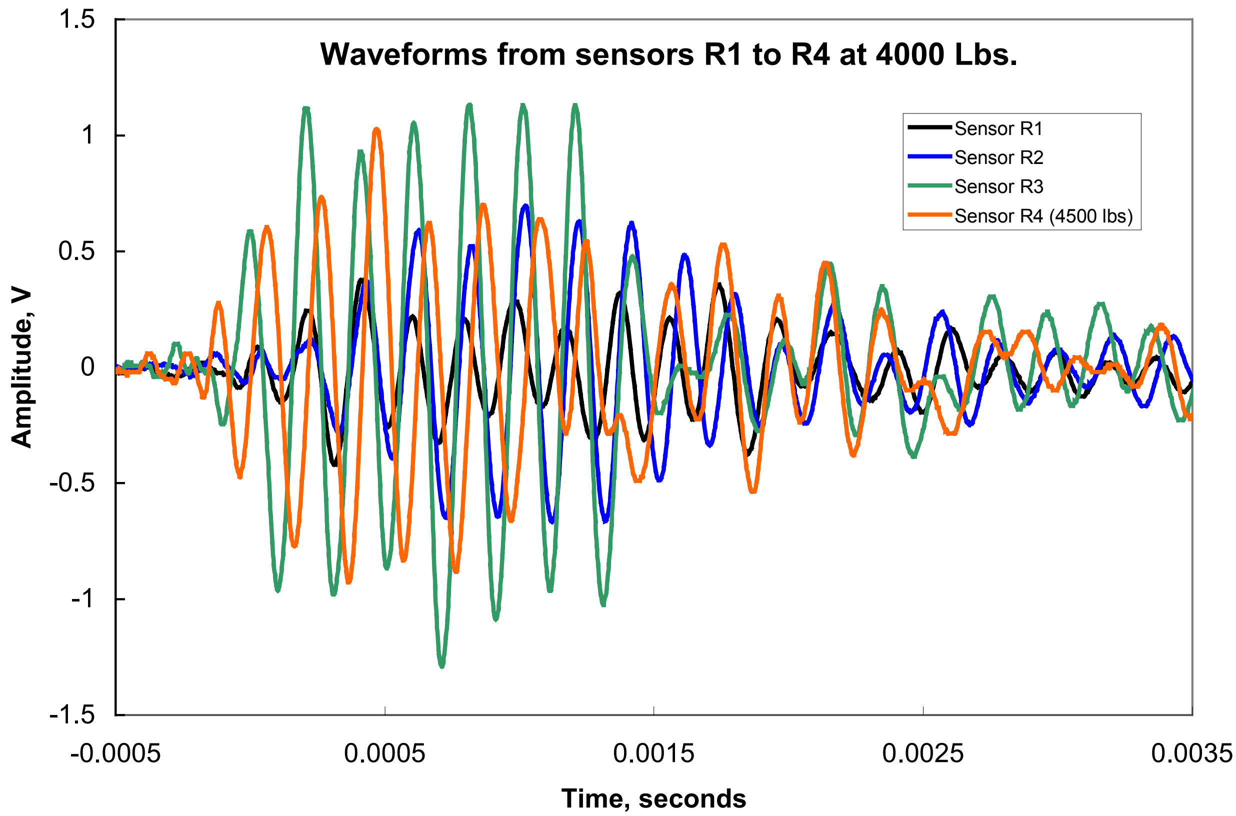


**Figure 12. Comparison of waveforms from sensors R1 to R4 at 4000–4500-lb. loads**

### *4.1 Resonant Comparison Analysis*

One way of detecting damage in an approximately symmetric structure using wave propagation or vibration is to use the resonant comparison method. In this approach, the exciting actuator is located at the center of a symmetric region. Sensors are symmetrically located on either side of the actuator to measure the response. Any unsymmetrical damage growing in this region can be identified from a comparison of the signals from the two sensors. The method compares responses of symmetrically placed sensors at resonance to detect damage using minimal historical data from the healthy structure. The damage indicator is defined as:

$$
\begin{aligned}
d_{ij} &= \left(\Delta_{ij}^{h} - \Delta_{ij}\right) / \Delta_{ij}^{h} \\
\Delta_{ij} &= \max\left|(x_i(t) - x_j(t))\right| \qquad (1) \\
\Delta_{ij}^{h} &= \max\left|(x_i^{h}(t) - x_j^{h}(t))\right|
\end{aligned}
$$

where $x_i(t)$ is a displacement or strain response variable from the structure, $\Delta_{ij}$ is the maximum of the difference in time domain responses at sensors *i* and *j,* and the superscript *h* represents the healthy response. The method is used here with a tone burst input.

Plots of the difference in responses R1-R2 and R3-R4 for the no load and 4500-lb load conditions are shown in Figure 13a together. Figure 13b separates the results for clarity. These signals show a reduction in amplitude and small shift to the right at the 4000-lb. load level compared to the no load condition.

During the loading at 4000 lbs. the hold time was short and the data for receiver R4 could not be collected. Thus, data was collected for receiver R4 at 4500 lbs. and used in the analysis. This will put some error in the comparison of waveforms R3 and R4 and may make the damage indicator slightly larger. The signals show a change in amplitude and a phase shift to the right as the load level increases from the no load condition. This occurs for all receivers, except that at receiver R1, the phase shifts to the right at the beginning of the response and then shifts back to the left to become in-phase again. This, which only occurred in receiver R1, may be due to wave reflection between receiver R1 and the root end of the blade. The damage indicator values computed from these plots are $d_{12} = 0.96$ and $d_{34} = 0.06$. These values indicate a significant change in the structure due to damage and the change in geometry (bending). This damage indicator is based on the change in the peak amplitude of the difference in the response of pairs of receiver patches. A large change or damage is predicted between sensors R1 to R2 and a small change or damage between sensors R3 to R4. In future blade testing, more time must be allocated to perform a detailed pre-test survey of the wave propagation characteristics of the blade with the load saddles attached to help interpret the SHM results.

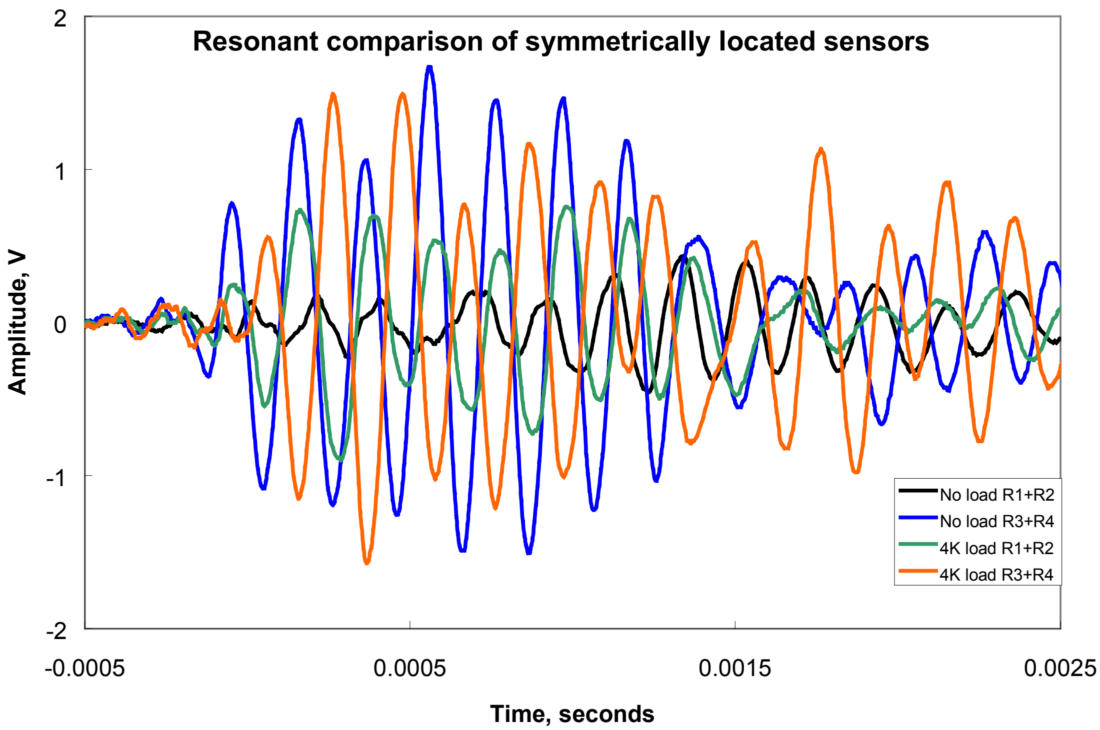


**Figure 13a. Resonant comparison of symmetrically located sensors at no load and 4000-lb. load**

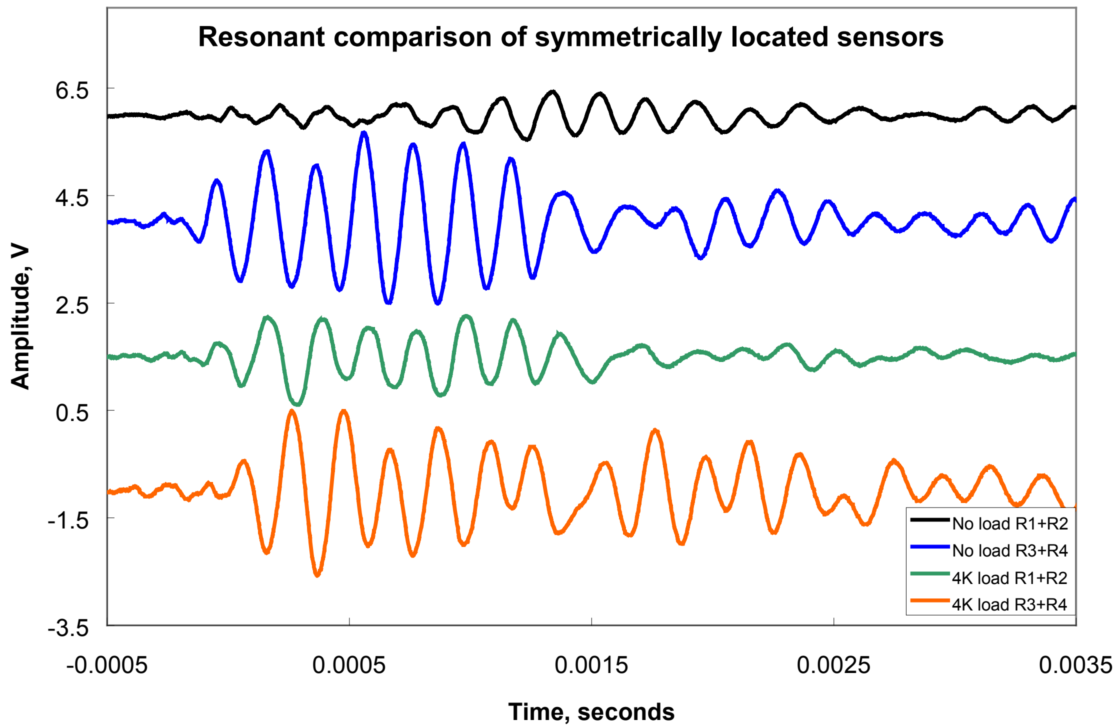


**Figure 13b. Resonant comparison of symmetrically located sensors at no load and 4000 lb. (4500 lbs. for R4) load with the waveforms separated along the vertical axis for clarity**

**Table 1. Resonant Comparison Results of the Sensors in Regions A and B**

| Resonant comparison of symmetrically located sensors - damage based on peak amplitudes | | | | | |
|---|---|---|---|---|---|
| R1 + R2 | | | R3+R4 | | |
| No Load | 4000 Lbs. Load | Damage Indicator | No Load | 4000 Lbs. Load | Damage Indicator |
| 0.46 | 0.90 | 0.96 | 1.67 | 1.57 | 0.06 |

### *4.2 Variance Analysis*

The variance damage index $d_i$ is used to quantify the damage detected at the *ith* sensor. This is computed as the square of the healthy, minus damaged vibration signals, normalized by the variance of the healthy signal (assuming the mean is zero). The damage indicator is computed as:

$$d_i = \frac{\int_{t1}^{t2} \left[ x_i^h(t) - x_i^d(t) \right]^2 dt}{\int_{t1}^{t2} \left[ x_i^h(t) \right]^2 dt} \tag{2}$$

where $x_i^h(t)$ is the voltage from the PZT $i$ in the healthy case, the subscript $h$ is the response from the healthy structure, and $t$ is time. The variance damage indicator is computed for the four sensors and the result is plotted in Figure 14. The response of the four sensors increases in amplitude with loading. Sensor responses are greater the farther the sensor is from the fixed end of the blade. This is most likely due to the increasing flexibility of the blade toward the free end. As the load increases, the receiver responses R1 and R2 diverge while the sensor responses R3 and R4 stay close together. The sensor responses R3 and R4 cross and drop below the response of R2 when the level reaches above approximately 3300 lbs. We hypothesize that the receiver responses R1 and R2 diverge because damage is occurring between them. The responses from receivers R2, R3 and R4 are similar because they are on one side of the damage area while the receiver R1 is on the other side of the damage area. It is important to note that the actual buckling occurred between receivers R1 and R2. The effect of compressive and buckling loading on the propagation of stress waves in a composite shell structure is unknown. We recommend that flat composite plates be tested in a material testing system (MTS) machine under compressive buckling loading. Stress waves can then be propagated in the plate to failure. This would provide a better understanding of damage propagation and allow the health monitoring sensor system to be optimized to sense this type of damage. Further testing at the NREL is needed to develop the health monitoring techniques specifically for wind turbine blades.

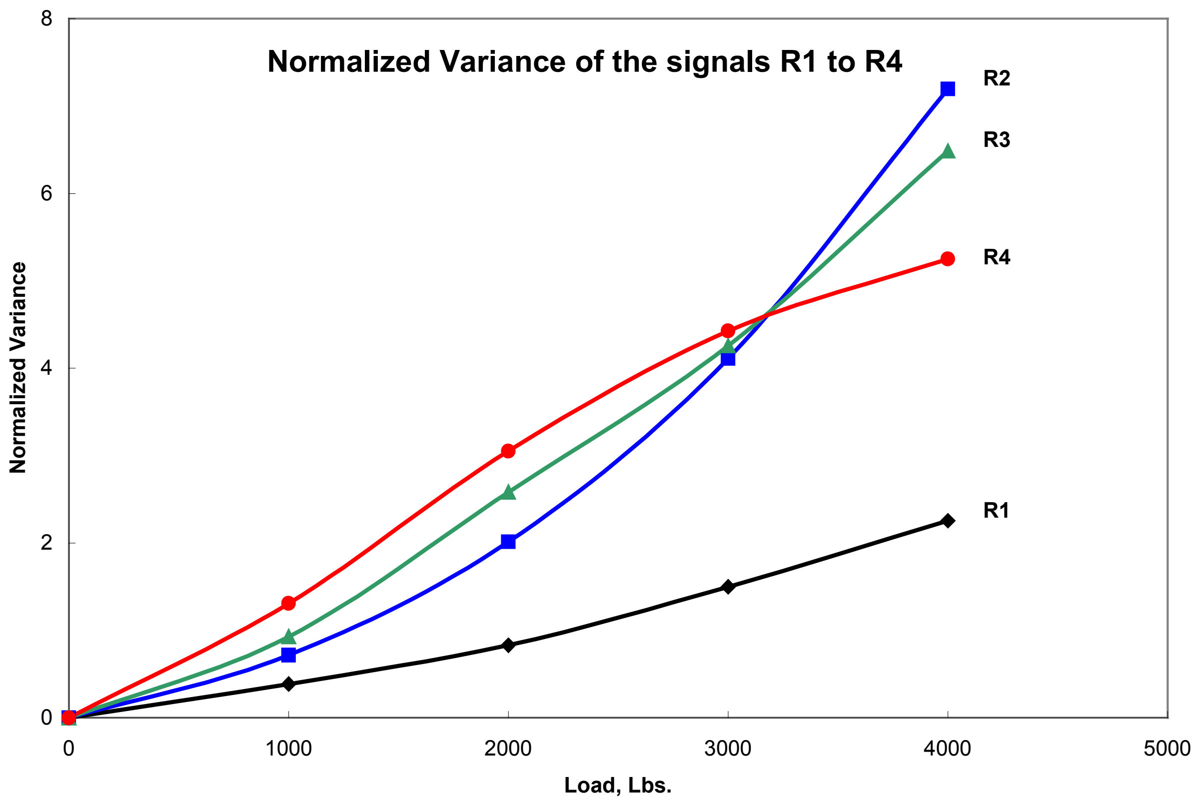


**Figure 14. Variance damage indicator for each sensor**

## 4.3 *Wavelet Pattern Recognition Analysis*

Figure 6a shows a phase and frequency shift in the response of sensor R1 between the no load and 4000-lb. load conditions. This time dependent frequency modulation of the signal has been examined in the time domain using the resonant comparison and variance methods. In the frequency domain, this modulation tends to be smeared by the Fourier transform. Time-frequency methods such as the short-time Fourier transform and the bilinear transform Wigner-Ville distribution, produce interference in the time and frequency domain (Note: W.J. Staszewski, refs. 41-42, provided much of the discussion on wavelets). This interference can be removed using different types of windows (kernels) - e.g. the Choi-Williams distribution. However, the smoothing procedure can lead to the removal of desired features. Wavelet analysis, which is a linear transformation, is able to resolve time dependent variations without interference. However, the Fourier analysis is a more straightforward analysis. An infinite number of different wavelets within both discrete and continuous wavelets classes raise the important question of which wavelets to choose for a specific signal. The most appropriate wavelets to use for damage detection is a topic currently under investigation at NCA&T and elsewhere. Some guidance based on regularity, vanishing moments, and time-frequency localization of wavelets can be considered. In general, continuous wavelets are better for time-frequency analysis while discrete wavelets are more suitable for decomposition, compression, and feature selection. However, the choice is not always clear. The continuous wavelets transform as signal decomposition that cannot be directly compared to any time-frequency representation. However, there is an inverse relationship between a scale parameter and the central frequency of the wavelet filter. The wavelet map indicates the presence of a particular scale versus time. The scale can be related to the inverse of frequency. This relationship between frequency and scale is useful to understanding the effects of damage on the signal.

The Mexican Hat wavelet was used in the present analysis to detect damage in the blade. This wavelet function (Fig. 15) is derived from a function that is proportional to the second derivative of the Gaussian probability density function. The excitation or reference signal at transmitter T1, and the resultant stress wave signals from sensor R1 at the no load, and 4000-lb. load conditions are shown in Figure 16. The wavelet transform is first performed on the excitation signal for reference and for understanding the characteristics of the transform (Figure 17). The wavelet transformation is then performed on the response R1 signal in the no load condition (Figure 18), to be used as the healthy or historical pattern, and for the response R1 signal at the 4000-lb. load condition (Figure 19). A comparison of the wavelet maps for the response R1 in the healthy and loaded condition show a difference in patterns. This difference indicates a change in the blade structural properties or damage. The time points in Figures 17-19 correspond to the time scale in Figure 16. Referring to Figures 18 and 19, the wavelet scale magnitude is changed in the region of time points from 250 to 450 and at scales from 17 to 31. These results show that the tone burst from exciter T1 is sent through the blade and is modified by the blade structure between the exciter T1 and receiver R1. This process changes the distribution of energy at higher scales of the wavelet. A more quantitative means of classifying the damage using wavelets is being investigated.

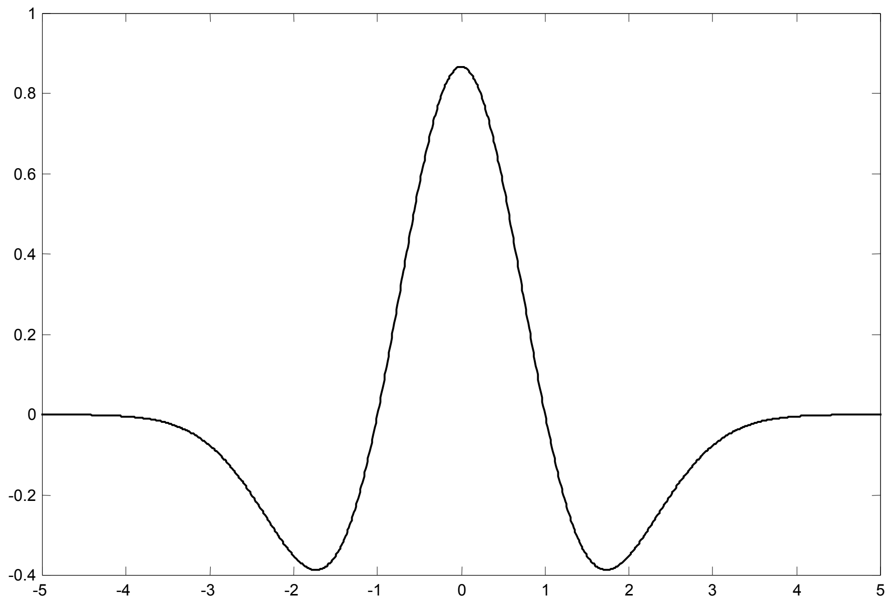


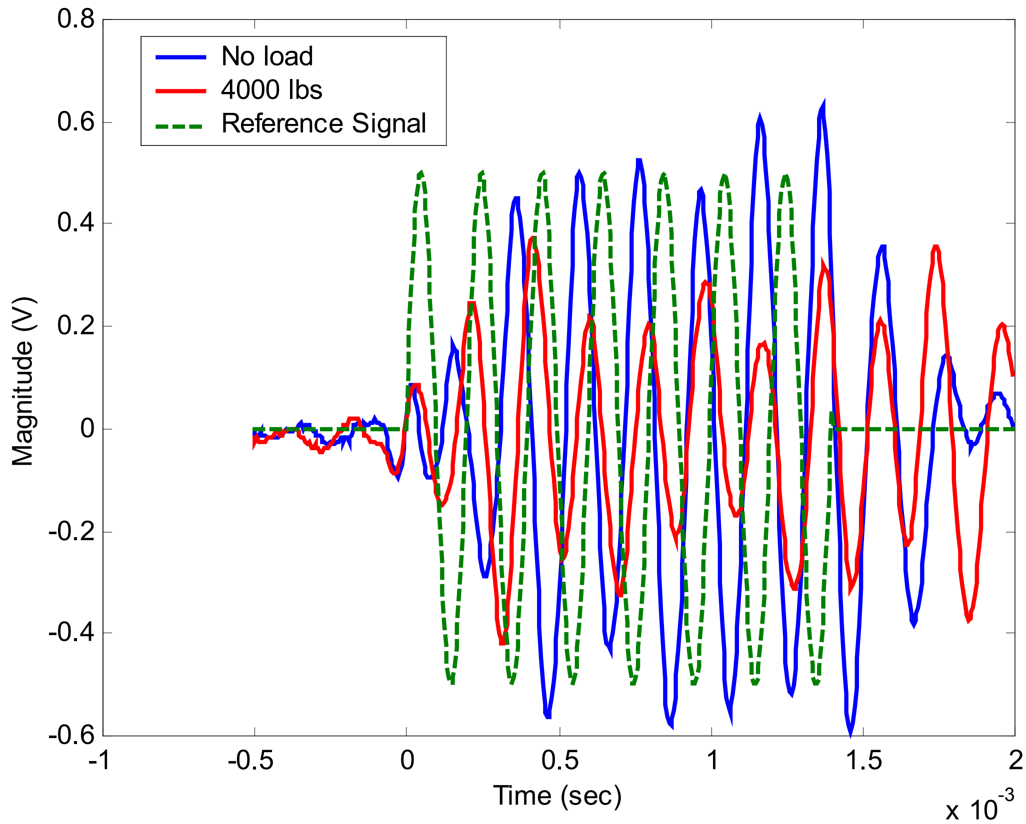


**Figure 16. The excitation or reference signal at transmitter T1 and the resultant stress wave signals from sensor R1 at the no load and 4000-lb load conditions**

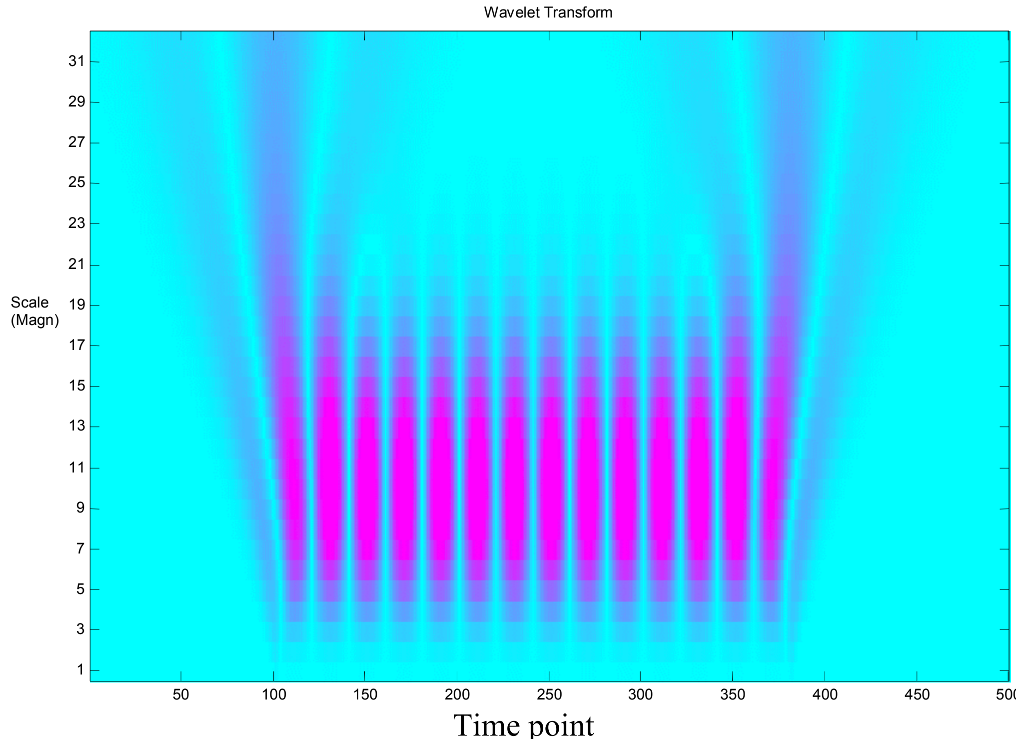


**Figure 17. Wavelet transform of the excitation sine burst signal**

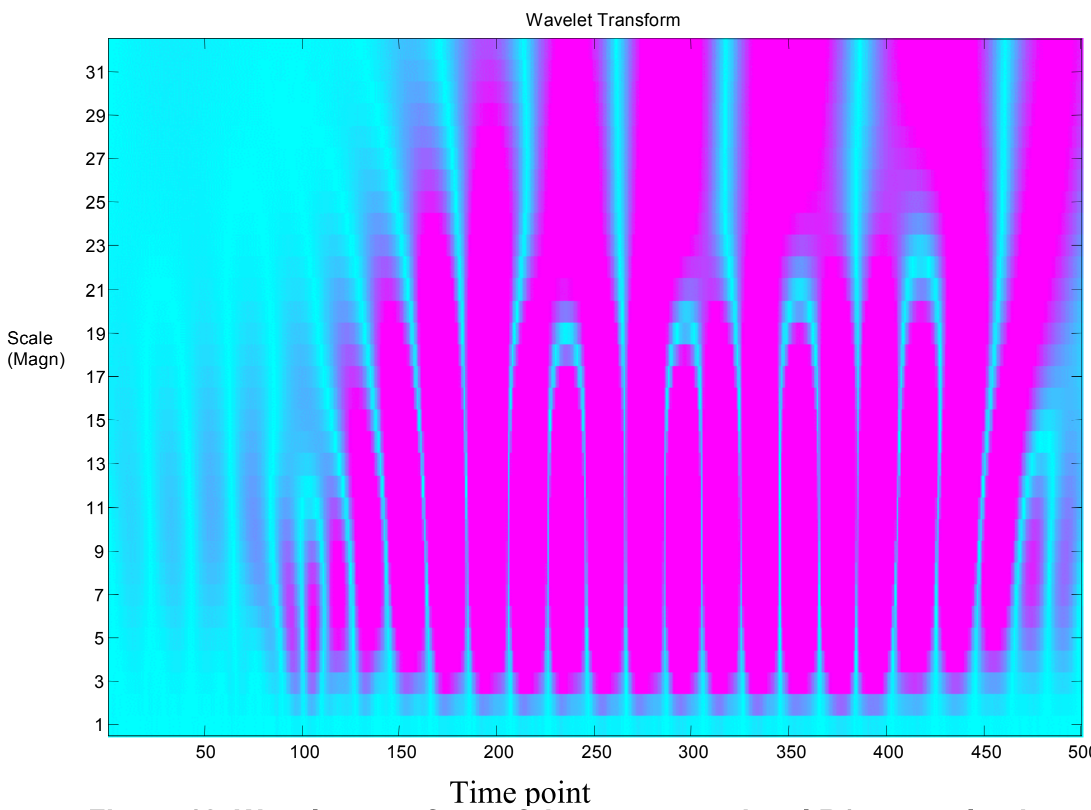


**Figure 18. Wavelet transform of the response signal R1 at zero load**

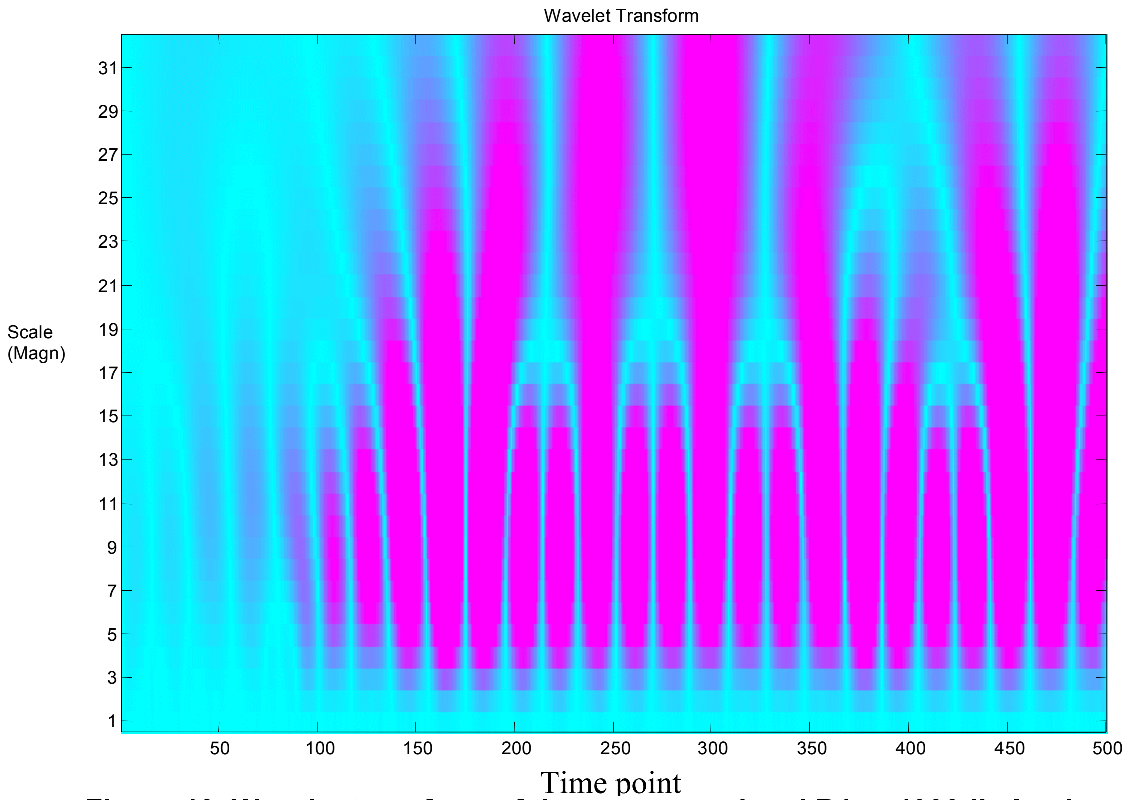


**Figure 19. Wavelet transform of the response signal R1 at 4000-lb. load**

# 5.0 Post-Failure Analyses

Failure origin in wind turbine blades should be determined to confidently redesign the blades for increased strength. It is not possible to trace fracture origins on failed composite material parts as can be done with many homogeneous materials [55]. Neither is it possible to distinguish fatigue fractures from static overload cases. Only in the case of stress corrosion cracks is fractography analysis useful. Generally, some combination of detailed stress analysis (like FEA) and/or careful observation during the test prior to failure is necessary.

While typical fractography analysis cannot be applied, limited information regarding the failure mode of the blade was gathered from the cross section of the blade at the failure location (Figure 20). Figure 21 shows the cross section of the blade immediately to the left of the failure location. Figure 22 shows the cross section of the shear web, and Figure 23 shows the top portion at a higher magnification. Of particular interest is the shear web, because failure of the blade shown in Figure 20 is likely to have been preceded by buckling of the shear web. Several features may be noted in Figure 22. The channel shaped web section is damaged. Delaminations between layers are evident in the cross section of the web in both the top of the vertical portion and in the top flange. The web portion of the channel section that is expected to be straight and normal to the base has a bent portion at the top. Because the adhesive bond between the web and top skin of the blade is still undamaged, it appears that the bend in the web section was present in the fabricated blade. Such deviations in the geometry and alignment are likely to reduce the buckling strength of the blade significantly. The delaminations in different parts of the web can also be seen in the side views of the web (shown in Figures 24 and 25 as bright patches). The buckling of the web likely causes these delaminations. Figure 25 shows wider damage to the web beyond the delaminations shown in the preceding figures. There is a difference in the translucency in the web as indicated by the difference in the shades between the two regions shown by the arrows. The portion of the web having the lighter shade became less translucent, probably because of the appearance of micro cracks in the web that resulted from the buckling of the shear web. Figure 26 shows the leading edge of the blade. The complete separation of the top and bottom portions of the leading edge of the blade is evident. The lack of penetration of the crack into either of the two parts suggests the bond is the weak link between the two surfaces. Changes in the web and bond design may increase the buckling strength of the blade, but the manufacturing and cost implications of the changes are not considered here.

The different types of damage occurring in a wind turbine blade and the locations of the damage might be determined by a structural health monitoring sensor system integrated inside the blade. This would provide information useful for preventing catastrophic failure of the blade and for redesigning weak areas of the blade.

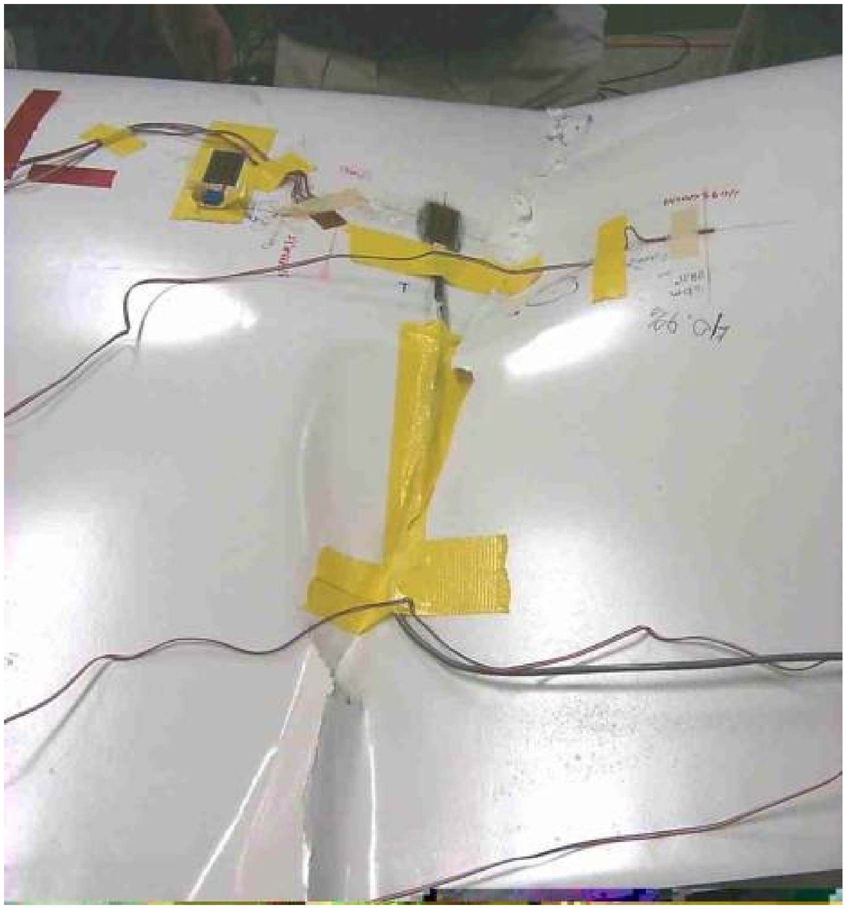

**Figure 20. Failure region of the wind turbine blade**

**Figure 21. A segment of the blade corresponding to the left half of the buckling region shown in Figure 20**

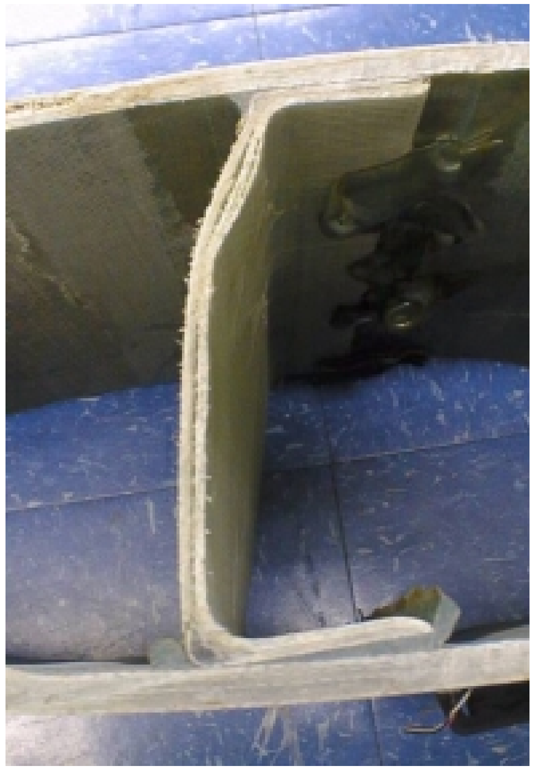

**Figure 22. Cross-section of the web near the location of buckling of the blade**

**Figure 23. Enlarged view showing delaminations in the web and in the flange portion of the channel section**

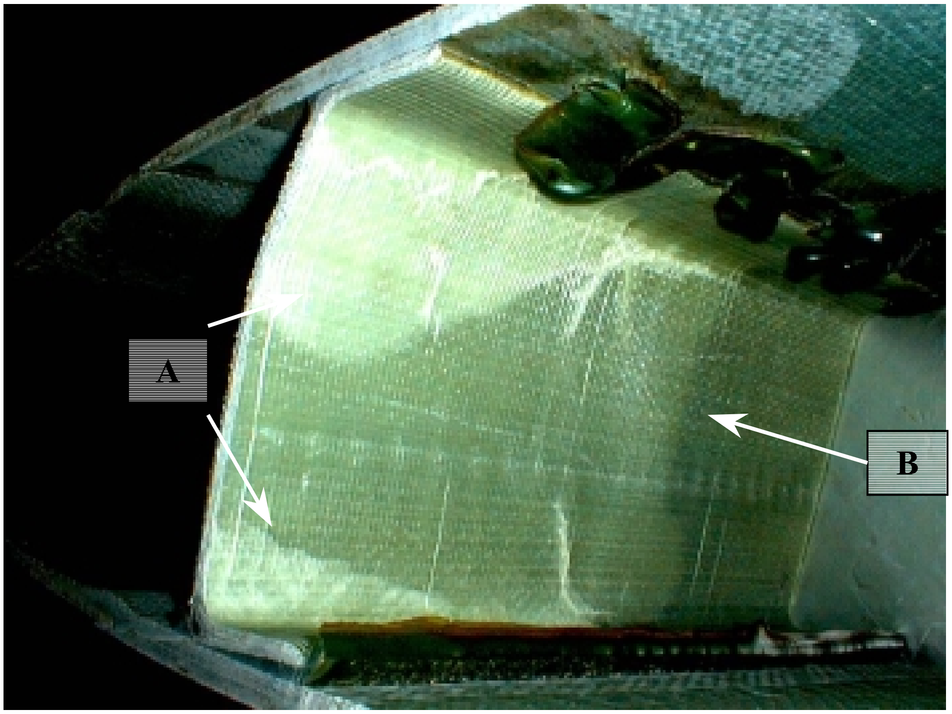


**Figure 24. Right side of the web showing delaminations (A) at the top and bottom portions of the web, and (B) the vertical line separating the relatively opaque region and the translucent region of the web**

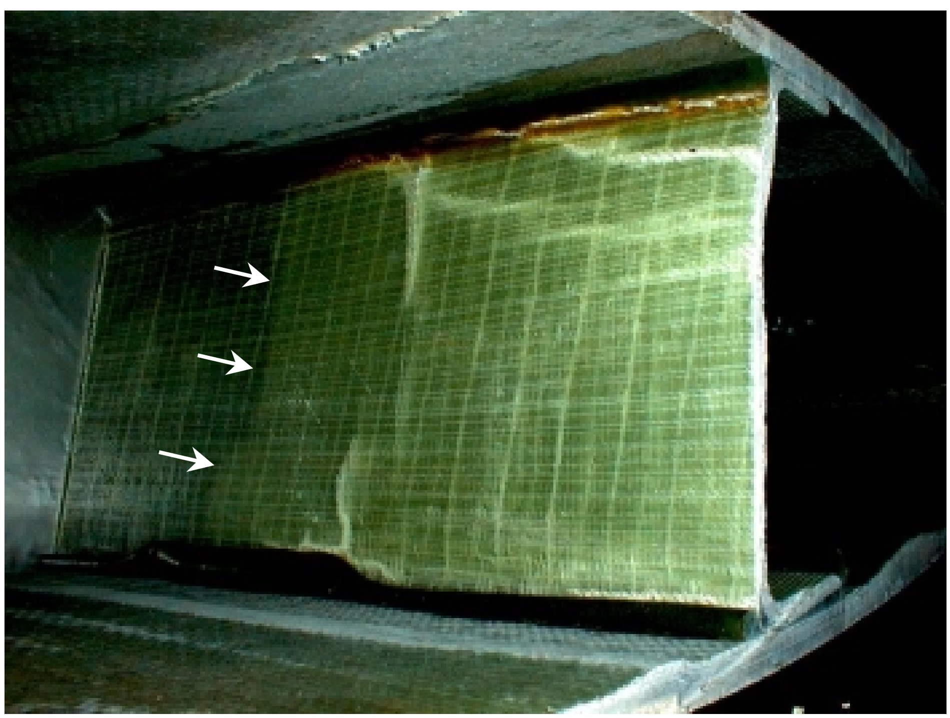

**Figure 25. Left side of the web showing the damage and the vertical line separating the relatively opaque region and the translucent region of the web as shown by the arrows**

**Figure 26. The leading edge of the blade showing separation of the top and bottom skins**

# 6.0 Conclusions

In a preliminary investigation, the structural change and damage occurring to the ERS-0100 wind turbine blade during the loading cycle was monitored through propagating stress waves. Bonded PZT patches were used for generating and receiving the stress waves. The wind turbine blade failed by local buckling at 37.5% blade length measured from the root end, at a load level of 5500 lbs. Readings were obtained only up to a load level of 4000 lbs. for three of the sensors, and 4500 lbs. for the other sensor. These limitations were due to constraints imposed by the required minimum loading rate specified for this test. Of the four sensors, the signals from receivers R1 and R2 showed the largest changes in the stress wave parameters. The R1 and R2 sensors were located across the damage region and were able to identify the occurrence and bound the location of damage. Hence, stress wave propagation appears to have a promising potential for the detection of evolving damage in composite structures such as wind turbine blades.

The goal of the NREL and NCA&T health monitoring research program is to develop a simple, low-cost, reliable sensor system to monitor the condition of wind turbine blades. This system can be embedded into wind turbine blades during manufacturing, and will warn of blade failure for 10–20 years of service. Testing of health monitoring systems at the NREL, as described in this report, is a necessary and very important part of the development of a *"smart blade"* for wind turbines.

# 7.0 Recommendations

Based on what was learned in the testing described in this report and developments in the NCA&T Laboratory, recommendations for further steps in the development of the *"smart blade"* are made here.

1. Laboratory tests on simpler structures, such as plates under compressive loading, should be performed to verify the sensitivity of the propagating stress waves to structural damage [43-47]. The PZT patches could be optimized to launch stress waves of appropriate frequency. The effect of high stresses on the sensors must also be evaluated as the piezoceramic patches can fail in high stress regions.

2. Changes in the signal shape and the data acquisition procedure should be made to increase the accuracy and depth of information that is gathered during the experiments. Examples include triggering the data acquisition by the transmitted signal, the use of chirp and impulse signals instead of constant frequency tone bursts, optimizing the excitation frequency to minimize dispersion of the waves, and optimizing the sensor spacing and size.

3. A detailed failure analysis of the blade would help to correlate the changes in the stress waves with the local failure modes of the blade. If the health monitoring system could indicate the failure progression, this information could be used to improve the design of the blade.

4. A new sensor design using active composite fibers (patent application in process) is being developed at NCA&T [48-54] and should be tested at NREL. This sensor (standard patch is shown in Fig. 20) is a continuous distributed sensor and can be used for active interrogation or passive listening for damage. The larger coverage of this sensor would provide a better indication of damage location. The higher strain capability of the active fiber composite sensor allows it to be used on both sides of the blade, whereas the monolithic piezoceramic patches used in this test may fail in tension loading.

5. The SHM sensor should be embedded within a blade during manufacture and the blade should be tested to failure. The sensor design should be optimized and another blade with the embedded sensor built and put into the field and monitored in real-time using a LABVIEW system. This project should involve the same NCA&T, NREL, and Sandia personnel that performed the testing and research in this report.

6. This test uncovered some important factors in designing structural health monitoring systems. It indicated that measured stress waves are affected by; (1) the change in curvature of the structure; (2) the strain state in the sensors, actuators, and structure; (3) damage in the structure, and (4) that failure of the structure by buckling is a failure mode that may have not been investigated before using SHM techniques. Furthermore, research in this project may lead to a new area of structural health monitoring we call buckling health monitoring (BHM). The concept of predicting buckling could have applications for wind turbines, panels of high-speed aircraft, columns, civil infrastructure, and other structures. NCA&T and NREL are in a position to lead BHM research. Modeling of buckling of a simple fiberglass bar and an experiment to determine the sensitivity of wave propagation to buckling parameters is in the beginning stage at NC&T.

**Figure 20. Active fiber composite patch 5.25x2.5x0.0085 inches**

# Acknowledgments

The experimental investigation was performed August 1999 at the NREL blade test facility in Golden, Colorado. The opportunity for using the NREL facilities and to participate in their experiments is gratefully acknowledged. Particular thanks go to Walter Musial and Scott Hughes of NREL. Funding for this project was from NREL grant number: XCX-7-16469-01, "Control and Health Monitoring of Variable Speed Wind Power Generation Systems." The technical monitor of the grant is Alan Laxson (Dr. Peter Tu for the first year). The authors would also like to thank Mark Rumsey of Sandia for his support of this research effort.

# References


1. Ghoshal, A.; Sundaresan, M. J.; Schulz, M. J.; Pai. P.F. "Structural Health Monitoring Techniques for Wind Turbine Blades," in press, *Journal of Industrial Aerodynamics and Wind Power Engineering*, special issue.
2. Schulz, M.J.; Pai, P.F.; Inman, D.J. "Health Monitoring and Active Control of Composite Structures using Piezoceramic Patches." *Composites B Journal*; Vol. 30B, Number 7, 1999; pp. 713-725.
3. Schulz, M.J.; Pai, P.F.; Naser, A.S.; Chung, J. H. "Locating Structural Damage Using Frequency Response Reference Functions," *Journal of Intelligent Materials Systems and Structures*. Vol. 9, No. 11, 1999; pp. 899-905.
4. Zhang, H.; Schulz, M.J.; Naser, A.S.; Ferguson, F.; Pai, P.F. "Structural Health Monitoring using Transmittance Functions," *Mechanical Systems and Signal Processing*. 1999; 13(5) pp. 765-787.
5. Thyagarajan, S.K.; Schulz, M.J.; Pai, P.F.; Chung, J. "Detecting Structural Damage using Frequency Response Functions," letter to the editor, *Journal of Sound and Vibration*, 210(1). February 12, 1998; pp. 162-170.
6. Schulz, M. J.; Ghoshal, A.; Sundaresan, M. J.; Ferguson, F.; Pai, P.F.; Chung, J. H. *Distributed Sensors for Health Monitoring of Composite Materials*. ACUN-2 International Composites Meeting, Composites In The Transportation Industry, University of New South Wales, Sydney, Australia, February 14-18, 2000.
7. Waldron, K.; Ghoshal, A.; Schulz, M. J.; Sundaresan, M. J.; Ferguson, F. *Structural Damage Detection Using Operational Deflection Shapes*. NASA URC-SC 2000 Conference, April 7-10, 2000, Nashville, Tennessee.
8. Mickens, T.; Schulz, M. J.; Sundaresan, M. J.; Ghoshal, A.; Ferguson, F. *Structural Health Monitoring Using The Resonant Comparison Method*. NASA URC-SC 2000 Conference. April 7-10, 2000, Nashville, Tennessee.
9. Ghoshal, A.; Harrison, J.; Sundaresan, M.J.; Schulz, M.J.; Pai, P.F. *Toward Intelligent Rotor Systems*. American Helicopter Society Annual Meeting. May 2000. Virginia Beach, Virginia.
10. Frank, P.; Si Jin, Pai; Schulz, M.J. *Structural Damage Detection Using A Scanning Laser Vibrometer*. American Helicopter Society Annual Meeting, May 2000, Virginia Beach, Virginia.
11. Schulz, M.J.; Sundaresan, M.J.; Ghoshal, A. *Active Fiber Composites for Structural Health Monitoring*. SPIE 7th international Symposium on Smart Materials and Structures, March 5-9, 1999.
12. Waldron, K.; Ghoshal, A.; Schulz, M.J.; Sundaresan, M.J.; Ferguson, F., Pai,. P.F.; Chung, J. H. *The Use of Operational Deflection Shapes for Structural Damage Detection*. IMAC XVIII, Feb. 7-10, 2000, San Antonio, Texas.
13. Sundaresan, M.J.; Ghoshal, A.; Schulz, M.J.; Ferguson, F.; Pai, P.F.; Chung, J.H. *Crack Detection Using a Scanning Laser Vibrometer*. Second International Conference on Structural Health Monitoring. Stanford University, Stanford, California. 1999.
14. Ghoshal, A.; Sundaresan, M.J.; Schulz, M.J.; Pai, P.F. *Damage Detection in Composite Structures using Vibration Measurements*. 6th International Conference on Composites Engineering. June 27-July 3, 1999. Orlando, Florida.
15. Sundaresan, M.J.; Ghoshal, A.; Schulz, M.J.; and Pai, P.F. *Acoustic Emission Sensing Using Piezoceramic and Active Fiber Composite Patches*. ASNT 1999 Fall Conference. Phoenix, Arizona. October 11–15, 1999.
16. Sundaresan, M.J.; Ghoshal, A.; Schulz, M.J.; Ferguson, F.; Pai, P.F.; Wilkerson, C. *Damage Detection using a Laser Vibrometer and Active Fiber Composite Patch*. 6th International Conference on Composites Engineering. June 27–July 3, 1999. Orlando, Florida.
17. Sundaresan, M.J.; Schulz, M.J.; Hill, J.; Wheater, E.A.; Ferguson, F.; Pai, P.F. *Damage Detection on a Wind Turbine Blade Section*. IMAC XVII Conference. Orlando, Florida. February 3–8, 1999.

18. Li, J.; Sundaresan, M.J.; Schulz, M.J.; Naser, A.S.; Pai, P.F.; Chung, J.*; Damage Detection on an Aircraft Panel using Vibration Measurements*. ICAST Conference. October 16–18, 1998. Boston, Massachusetts.
19. Martin, W.N.; Schulz, M.J.; Naser, A.S.; Pai, P.F.; Wilkerson, C. *Detecting Damage on Symmetric Structures using Vibration Measurements*. 5th International Conference on Composites Engineering. July 5–11, 1998. Las Vegas, Nevada.
20. Pai, P.F.; Young, L.G.; Schulz, M.J.; Tu, K.C. *A Hybrid Modeling Approach for Structural Health Monitoring*. 5th International Conference on Composites Engineering. July 5–11, 1998. Las Vegas, Nevada.
21. Schulz, M.J.; Naser, A.S.; Wori, L.; Pai, P.F. *Damage Detection in Composite Beams using Longitudional Vibration*. 5th International Conference on Composites Engineering. July 5–11, 1998. Las Vegas, Nevada.
22. Martin, W.N., Jr., Naser, A.S., Schulz, M.J., Turrentine, D.F., and Eley, S.M., "Health Monitoring of Aerospace Structures Using Symmetric Transmittance Functions," NASA URC-TC'98 Technical Conference Abstracts. Huntsville, Alabama, February 22-25, 1998; pp. 114-115.
23. Schulz, M.J., Pai, P.F., Naser, A.S., Thyagarajan, S.K., and Mickens, T.D., "A New Approach To Overcoming Spatial Aliasing In Structural Damage Detection," NASA URC Technical Conference, February 22-26, 1998, Huntsville, Alabama.
24. Hughes, D.R., Craft, W.J., Schulz, M.J., Naser, A.S., and Martin, W.N., "Damage Detection and Impact Testing on Laminated and Sandwich Composite Panels," NASA URC Technical Conference, February 22-26, 1998, Huntsville, Alabama.
25. Zhang, H., Naser, A.S., Schulz, M.J., and Pai, P.F., "Health Monitoring of Composite Beams Using Piezoceramic Patches And Curvature Transmittance Functions," ASCE (American Society of Civil Engineering) Engineering Mechanics Div., San Diego, California, May 17-20, 1998.
26. Schulz, M.J., Brannon, G.S., Naser, A.S., and Pai, P.F., "Structural Health Monitoring using Frequency Response Functions and Sparse Measurements," IMAC-XVI, February 2-5, 1998, Santa Barbara, CA.
27. Schulz, M.J., Naser, A.S., Pai, P.F., and Chung, J., "Locating Structural Damage Using Frequency Response Reference Functions and Curvatures," International Workshop on Structural Health Monitoring," September 18-20, 1997, Stanford University, Stanford, California.
28. Schulz, M.J., Naser, A.S., Pai, P.F., Martin, W.N., Turrentine, D., and Wilkierson, C., "Health Monitoring of Composite Material Structures Using A Vibrometry Technique," 4th International Conference on Composites Engineering, July 6-11, 1997, Hawaii.
29. Schulz, M.J., Pai, P.F., Abdelnaser, A.S., and Chung, J., "Structural Damage Detection Using Transmittance Functions," IMAC-XV Conference, Feb. 3-6, 1997, Orlando, Florida.
30. Schulz, M.J., Pai, P.F., and Abdelnaser, A.S., "Frequency Response Function Assignment Technique For Structural Damage Identification," IMAC-XIV Conference, February 12-15, 1996, Dearborn Michigan.
31. Lichtenwalner, P. F., Dunne, J. P., Becker, R. S., Baumann, E. W., "Active Damage Interrogation System for Structural Health Monitoring," Proceedings, SPIE Symposium on Smart Structures and Materials, San Diego, California, 1997.
32. Chang, F., "Structural Health Monitoring: demands and challenges," SPIE 7th International Symposium on Smart Structures and Materials, keynote paper 3990-17, March 5-9, 2000.
33. Sun, F., C.A. Rogers, and C. Liang, 1995. "Structural Frequency Response Function Acquisition Via Electric Impedance Measurement of Surface-Bonded Piezoelectric Sensor/Actuator", AIAA-95-1127-CP, pp. 3450-3458.
34. Schoess, J., Malver, F., Iyer, B., Kooyman, J., "Rotor Acoustic Monitoring System (RAMS)-A Fatigue Crack Detection System," American Helicopter Society (AHS) Forum 53, May 1, 1997, Virginia Beach, Virginia.
35. Prosser, W.H., Jackson, K.E., Kellas, S., Smith, B.T., McKeon, J., and Friedman, A., "Advanced Waveform Based Acoustic Emission Detection of Matrix Cracking in Composites," Materials

*Evaluation*, Vol. 53(9), September 1995; pp. 1052-1058.
36. Prosser, W.H., “Acoustic Emission Structural Health Monitoring,” *Nondestructive Evaluation Sciences Branch Aviation Safety NRA Meeting*, December, 17, 1998, internal document, NASA Langley Research Center.
37. Sundaresan, M. J., and Shankar, G., “The Use of AET for Classifying Failure Modes in Composite Materials,” *ASME Winter Annual Meeting, New Orleans, Louisiana, November 23, 1993.*
38. Seydel, R.E., Chang, F., "Implementation of a Real-Time Impact Identification Technique for Stiffened Composite Panels," *Proceedings of Second International Conference on Structural Health Monitoring, Stanford University, September 8-10, 1999;* pp. 225-233.
39. Wang, C.S., Chang, F., "Built-In Diagnostics for Impact Damage Identification of Composite Structures," *Proceeding of Second International Conference on Structural Health Monitoring, Stanford University, September 8-10, 1999;* pp. 612-621.
40. Active Control Experts, 215 First St., Cambridge, Massachusetts 02142.
41. Personal conversations with W.J. Staszewski, 3/2000.
42. W.J. Staszewski and G.R. Tomlinson, 1994, "Application of the wavelet transform to fault detection in a spur gear", *Mechanical Systems and Signal Processing*, Vol. 8, No. 3, pp. 289-307.
43. Achenbach, J.D., *Wave Propagation in Elastic Solids*, North Holland Publishing Company, 1973.
44. Ballentine, D.S., White, R.M., Martin, S.J., Ricco, A.J., Zellers, E.T., Frye, G.C., Wohltjen, H., *Acoustic Wave Sensors, Theory, Design and Physico-Chemical Applications,* Academic Press Inc., 1997.
45. Campbell, C.K., *Surface Acoustic Wave Devices for Mobile and Wireless Communications,* Academic Press 1997.
46. Schmerr, L.W. Jr., *Fundamentals of Ultrasonic Nondestructive Evaluation,* Plenum Press, 1998.
47. Wasley, R.J., *Stress Wave Propagation in Solids,* Marcel Dekker, Inc, New York, 1973.
48. Bent, A. A., Hagood, N. W., “Piezoelectric Fiber Composites with Interdigitated Electrodes,” *Journal of Intelligent Material Systems and Structures*, 8, 1998.
49. Bent, A. A., *Active Fiber Composites for Structural Actuation,* Ph.D. Thesis. MIT, January 1997.
50. Hagood, N.W., Pizzochero, A., “Residual Stiffness and Actuation Properties of Piezoelectric Composites: Theory and Experiment,” *J. Intelligent Material Systems and Structures*, 8, September 1997; pp.724-737.
51. Chee, C.Y.K., Tong, L., Steven, G.P., “A Review on the Modeling of Piezoelectric Sensors and Actuators Incorporated in Intelligent Structures,” *J. Intelligent Material Systems and Structures*, 9, January, 1998; pp. 3-19.
52. Dong, J.J. *A Continuum Mixture Theory of Wave Propagation in Axially Polarized Piezoelectric Fibrous Composites*, Ph.D. Dissertation. University of Cincinnati, 1993.
53. Continuum Control Corporation, 45 Manning Park, Billerica, Massachusetts 01821.
54. CeraNova Corporation, 101 Constitution Boulevard, Suite D, Franklin, Massachusetts 02038-2587.
55. Mandell, John, University of Montana, Personal Correspondence, johnm@coe.montana.edu, 8/4/00.

# Appendix

- **Photographs of blade and test equipment**

- **Plots of signals from sensors R1-R4 plotted for a longer duration and without overlap**

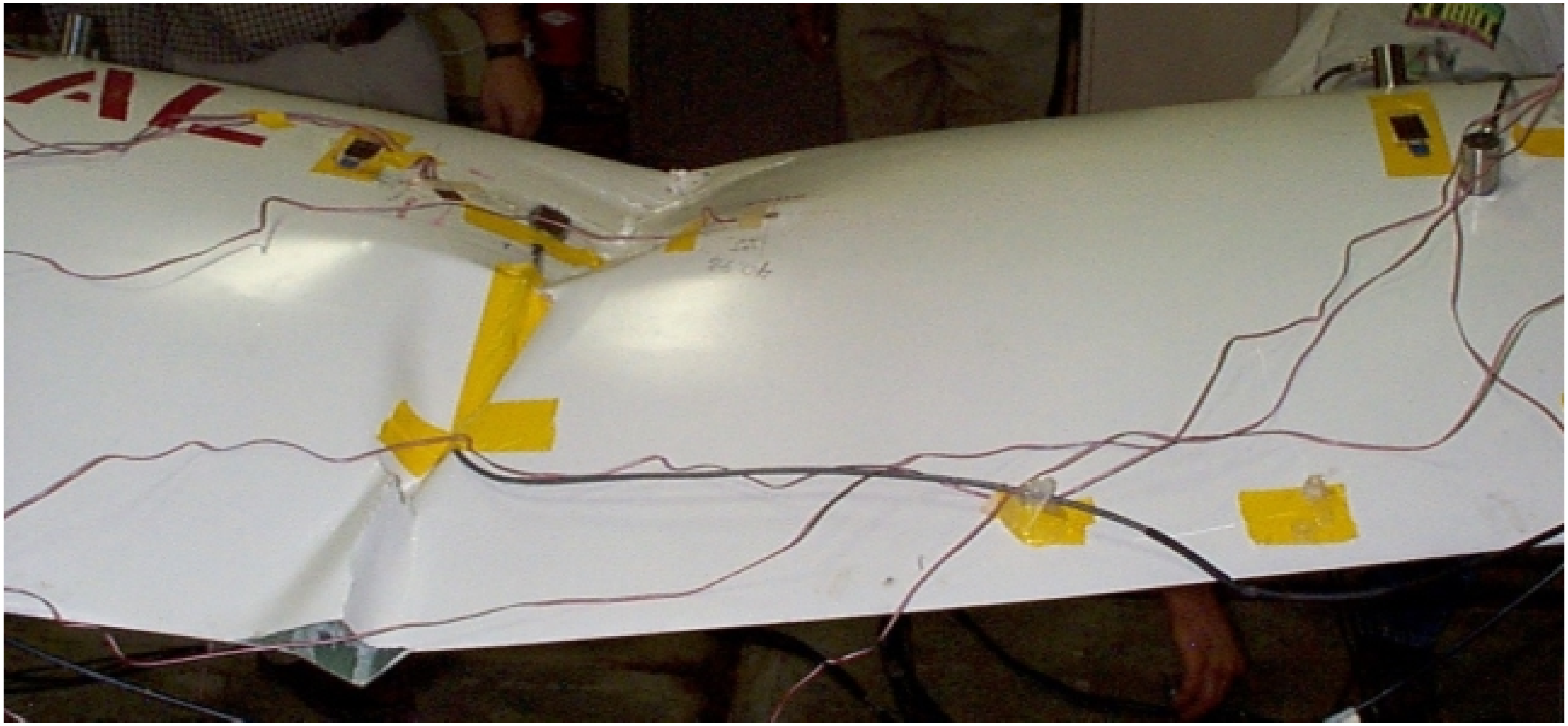

**Figure A.1. Close-up view of buckled region of blade**

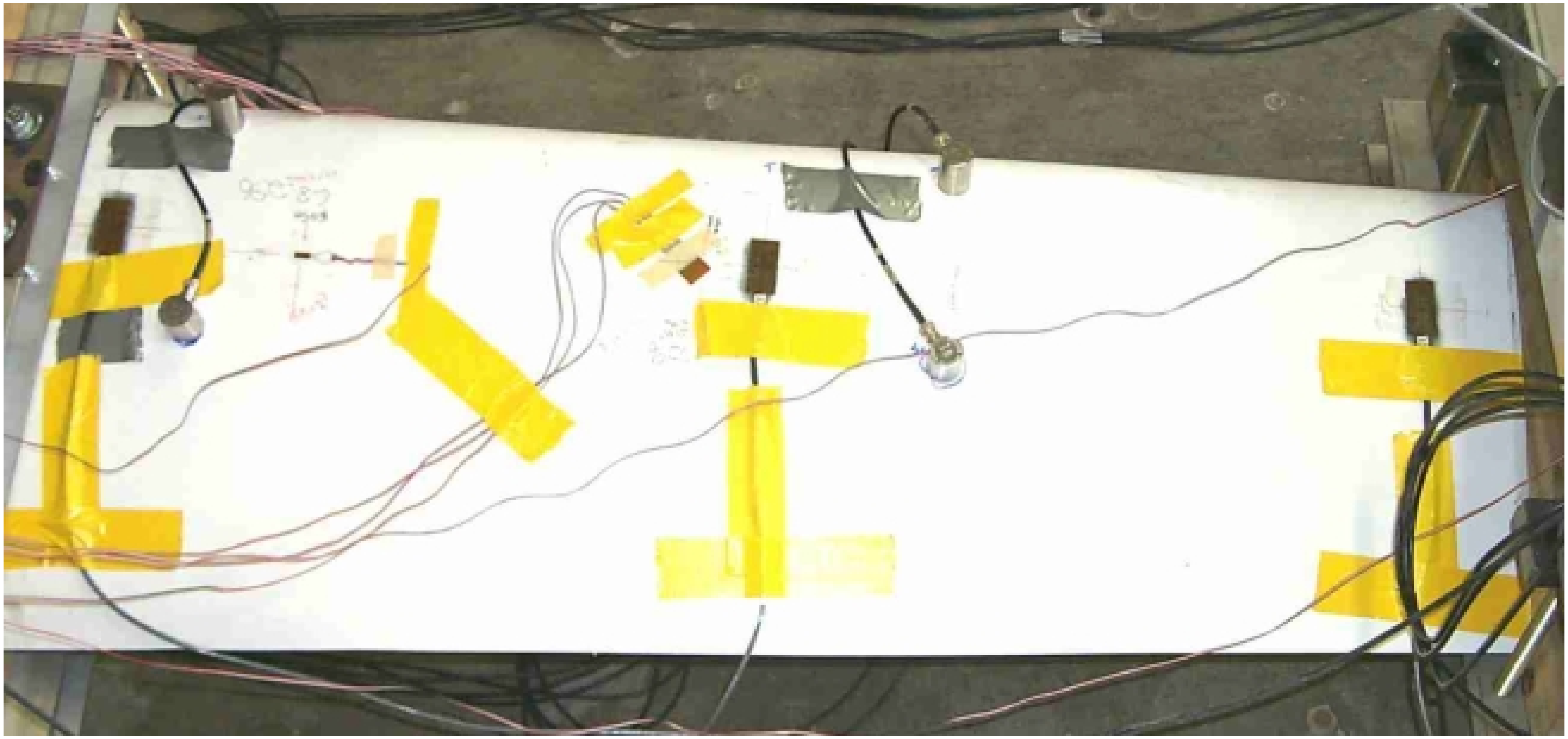

**Figure A.2. Acoustic emission, strain gage and PZT sensors on blade**


**Figure A.3. Field portable structural health monitoring instrumentation**

**Figure A.4. View of blade being installed**


**Figure A.5. View of blade after buckling**

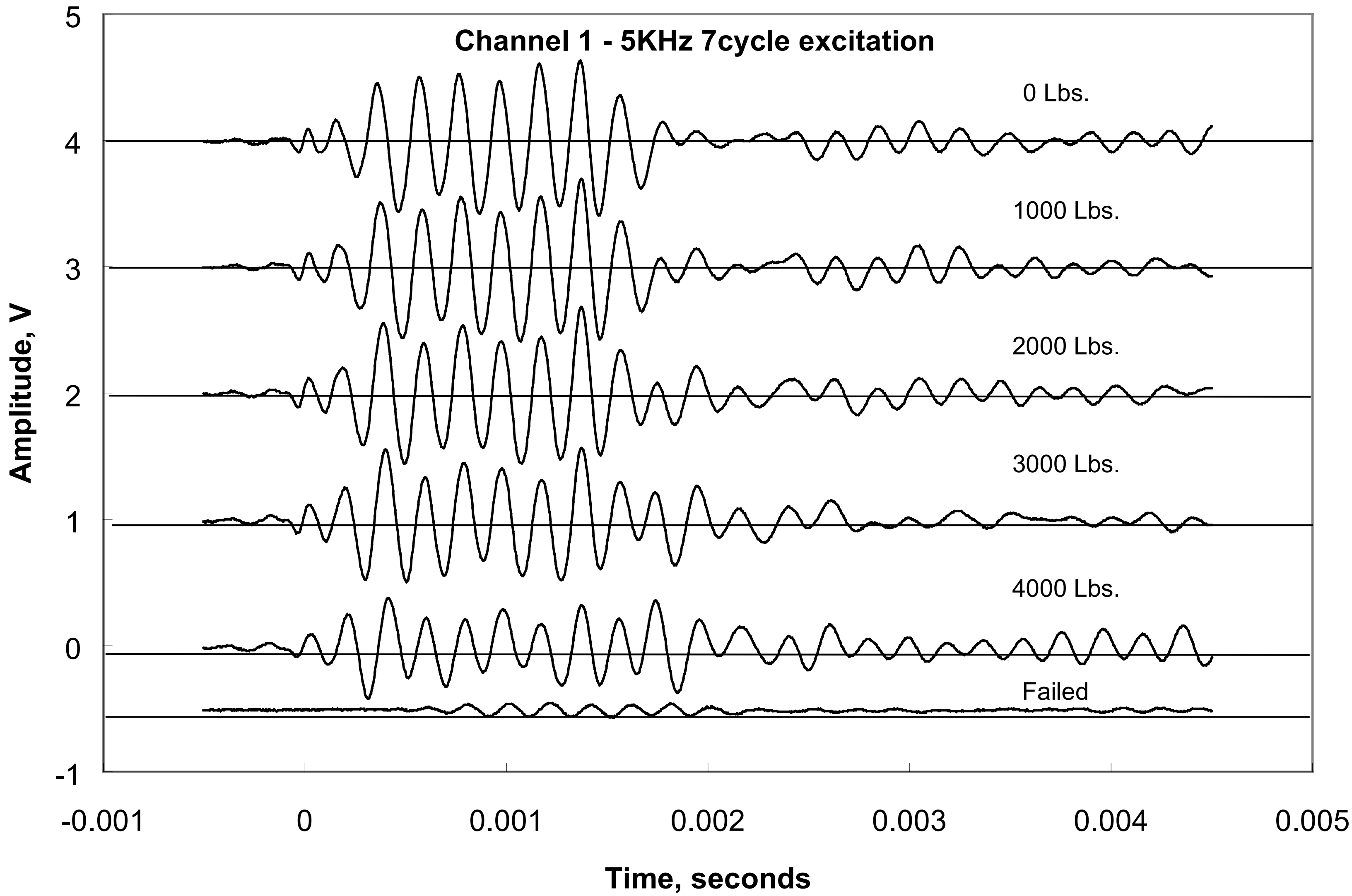


**Figure A.6. Signals from sensor R1 plotted for a longer duration and without overlap**

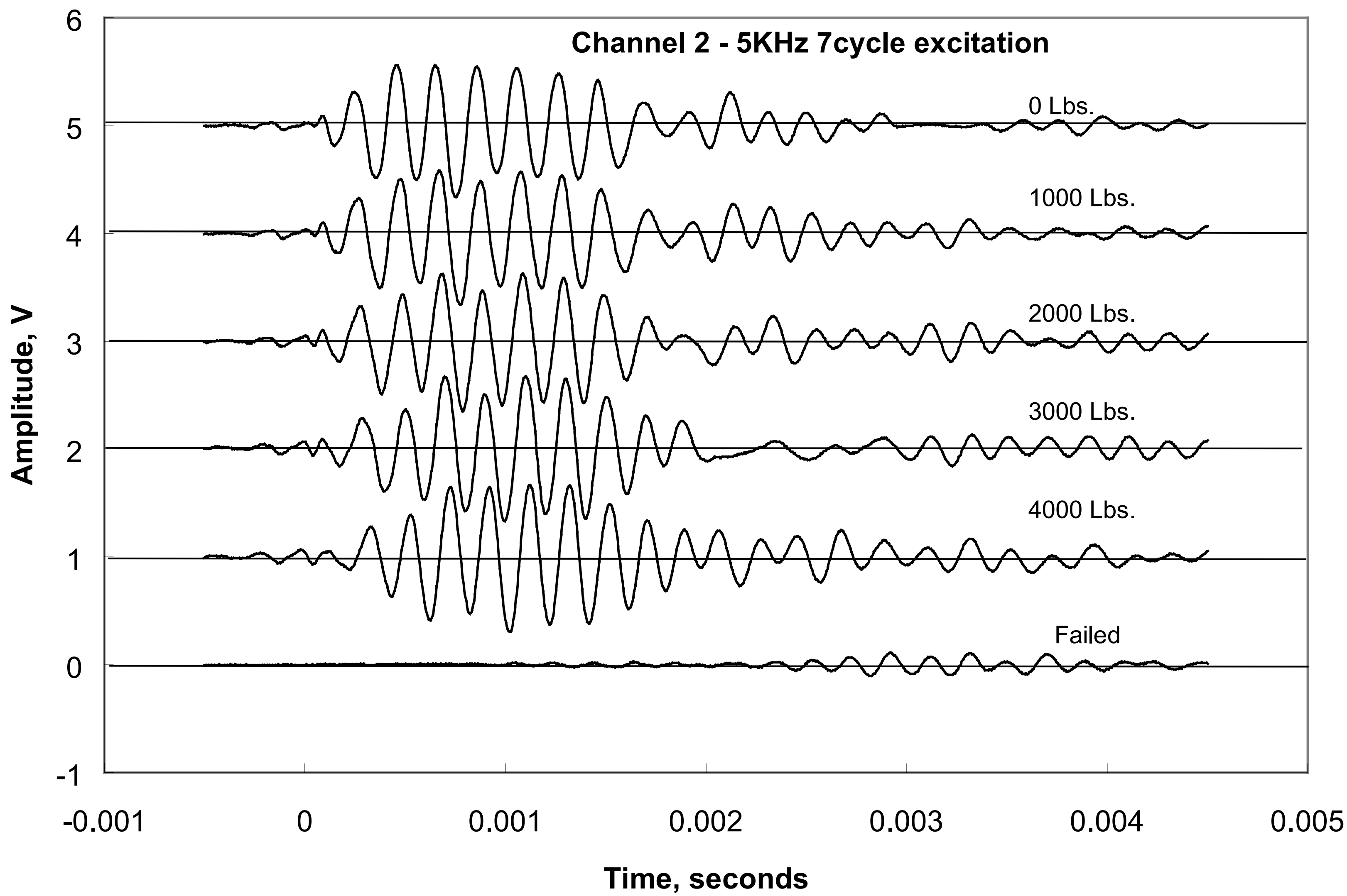


**Figure A.7. Signals from sensor R2 plotted for a longer duration and without overlap**

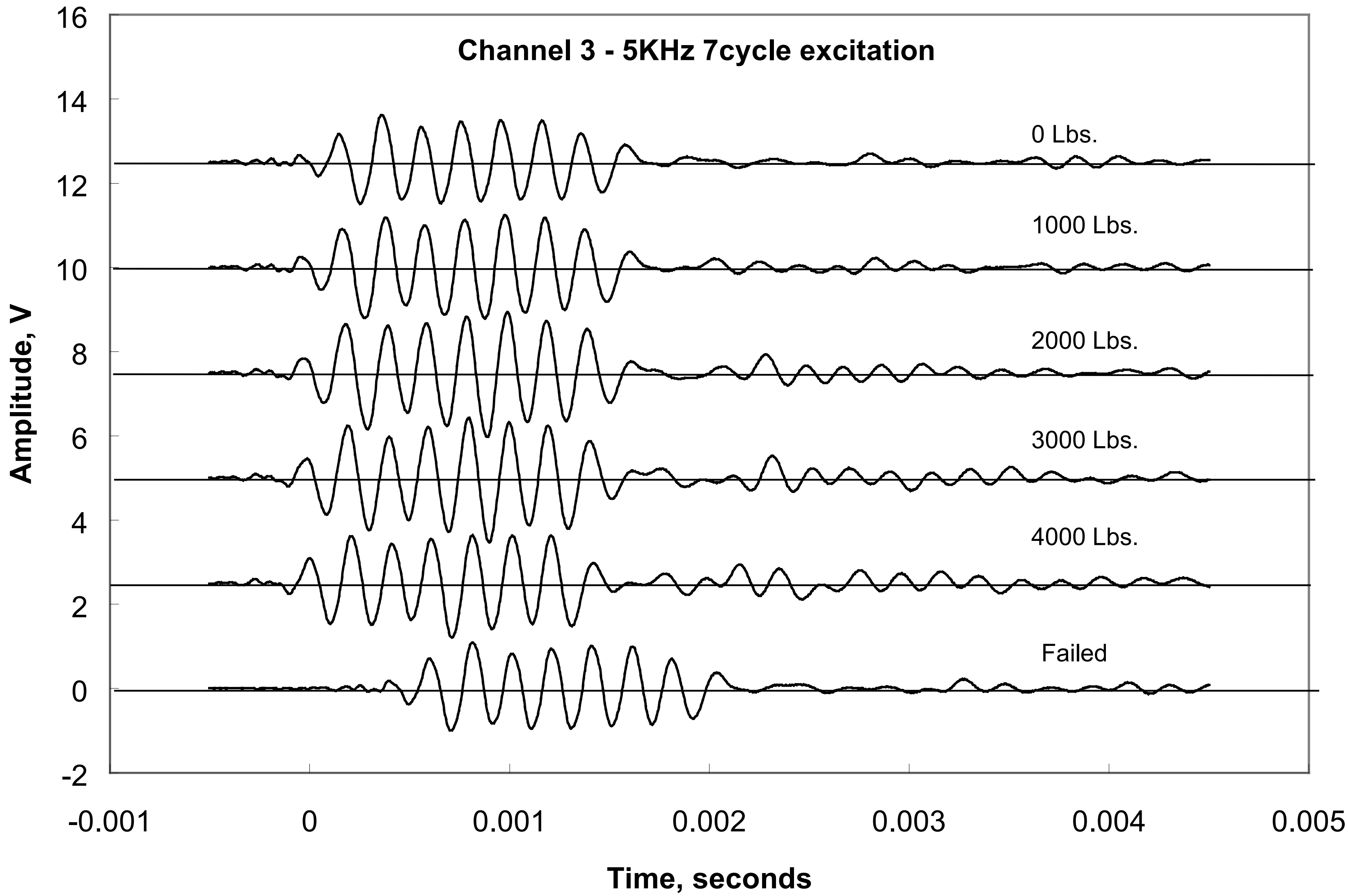


**Figure A.8. Signals from sensor R3 plotted for a longer duration and without overlap**

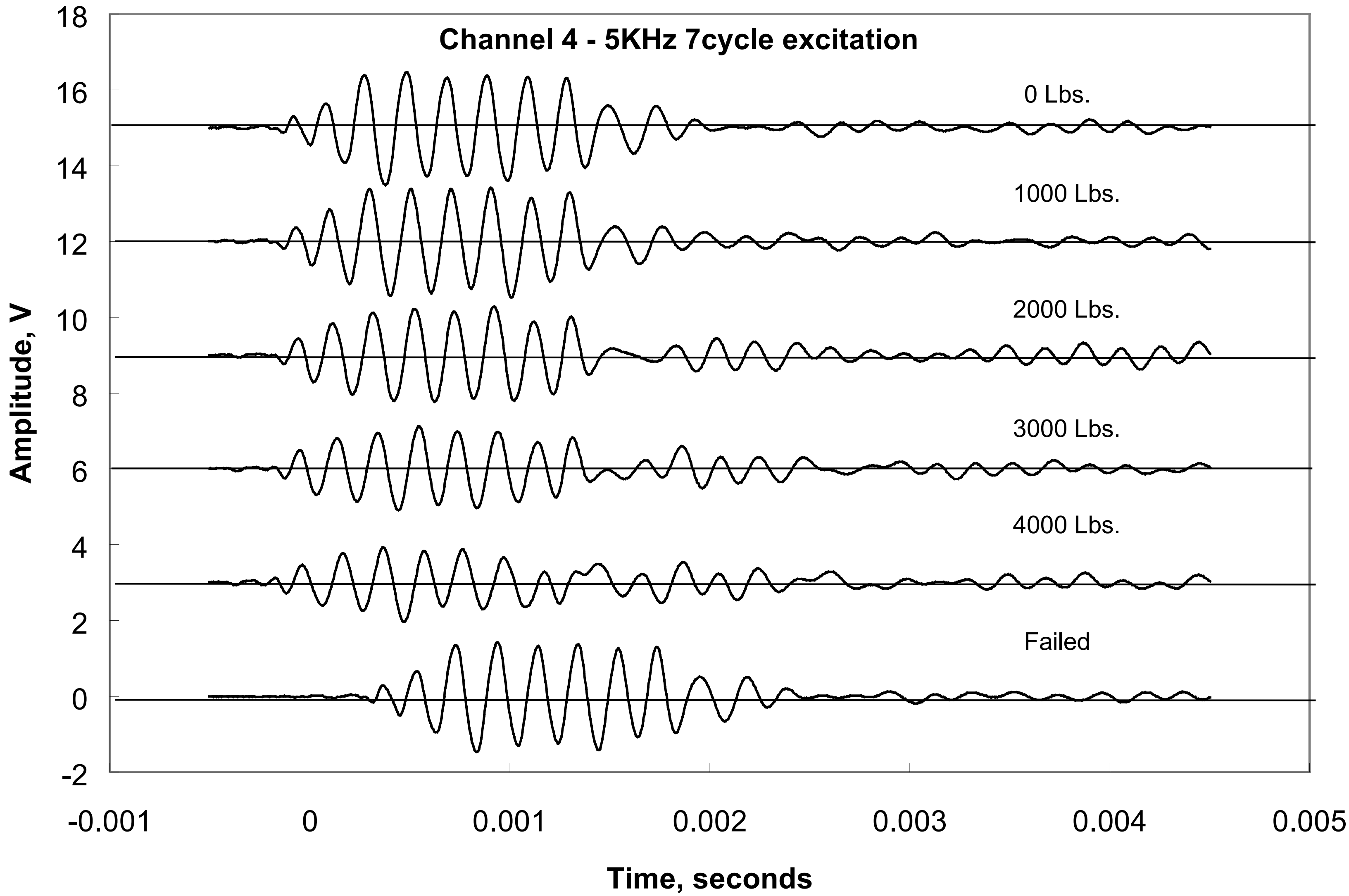


**Figure A.9. Signals from sensor R4 plotted for a longer duration and without overlap**

# REPORT DOCUMENTATION PAGE

*Form Approved*
*OMB NO. 0704-0188*



| 1. AGENCY USE ONLY (Leave blank) | 2. REPORT DATE | 3. REPORT TYPE AND DATES COVERED |
|---|---|---|
| | March 2002 | Subcontract Report |

4. TITLE AND SUBTITLE
Structural Health Monitoring Static Test of a Wind Turbine Blade: August 1999

5. FUNDING NUMBERS
WE00.1610

6. AUTHOR(S)
Mannur J. Sundaresan, Mark J. Schulz, and Anindya Ghoshal

7. PERFORMING ORGANIZATION NAME(S) AND ADDRESS(ES)
Intelligent Structures and Mechanisms (ISM) Laboratory
Department of Mechanical Engineering
North Carolina A&T State University
Greensboro, NC 27411

8. PERFORMING ORGANIZATION REPORT NUMBER

9. SPONSORING/MONITORING AGENCY NAME(S) AND ADDRESS(ES)
National Renewable Energy Laboratory
1617 Cole Blvd.
Golden, CO 80401-3393

10. SPONSORING/MONITORING AGENCY REPORT NUMBER
NREL/SR-500-28719

11. SUPPLEMENTARY NOTES
NREL Technical Monitor: Alan S. Laxson

12a. DISTRIBUTION/AVAILABILITY STATEMENT
National Technical Information Service
U.S. Department of Commerce
5285 Port Royal Road
Springfield, VA 22161

12b. DISTRIBUTION CODE

13. ABSTRACT *(Maximum 200 words)*
Structural health monitoring research is being performed by NCA&T, NREL, and Sandia to develop a "Smart Blade" with an embedded sensor system integrated into the blade by the manufacturer to continuously monitor the condition of the blade reducing or preventing fatigue damage. This will reduce maintenance costs and improve the reliability of wind power.

14. SUBJECT TERMS
wind turbine, wind energy, smart blade, wind power

15. NUMBER OF PAGES

16. PRICE CODE

| 17. SECURITY CLASSIFICATION OF REPORT | 18. SECURITY CLASSIFICATION OF THIS PAGE | 19. SECURITY CLASSIFICATION OF ABSTRACT | 20. LIMITATION OF ABSTRACT |
|---|---|---|---|
| Unclassified | Unclassified | Unclassified | UL |